

UNIVERSITÄTSKLINIKUM HAMBURG-EPPENDORF

Zentrum für Experimentelle Medizin
Institut für Zelluläre und Integrative Physiologie

Direktor: Prof. Dr. med. Heimo Ehmke

***KCND2* variants associated with global developmental delay differentially impair Kv4.2 channel gating**

Dissertation

zur Erlangung des Grades eines Doktors der Medizin
an der Medizinischen Fakultät der Universität Hamburg.

vorgelegt von:

Yongqiang Zhang

aus Nanjing, China

Hamburg 2021

(wird von der Medizinischen Fakultät ausgefüllt)

**Angenommen von der
Medizinischen Fakultät der Universität Hamburg am: 29.10.2021**

**Veröffentlicht mit Genehmigung der
Medizinischen Fakultät der Universität Hamburg.**

Prüfungsausschuss, der/die Vorsitzende: PD Dr. Thorsten Christ

Prüfungsausschuss, zweite/r Gutachter/in: Prof. Dr. Robert Bähring

Table of contents

1	Publication.....	1
1.1	Main paper.....	1
1.2	Supplementary material	40
1.3	Letter of acceptance	54
2	Presentation of the paper	55
2.1	Context of the study	55
2.1.1	Major new findings.....	55
2.1.2	Limitations of the study.....	59
2.1.3	Scientific and clinical outlook	61
2.2	References	63
3	Summary	65
4	Zusammenfassung	66
5	Declaration of own contribution.....	67
6	Acknowledgements.....	68
7	Curriculum Vitae	69
8	Eidesstattliche Versicherung.....	70

1 Publication

1.1 Main paper

(Accepted manuscript published in Human Molecular Genetics, 10 July 2021)

***KCND2* variants associated with
global developmental delay differentially impair Kv4.2 channel gating**

Yongqiang Zhang^{1,2}, Georgios Tachtsidis¹, Claudia Schob³, Mahmoud Koko⁴, Ulrike B.S. Hedrich⁴,
Holger Lerche⁴, Johannes R. Lemke⁵, Arie van Haeringen⁶, Claudia Ruivenkamp⁶, Trine Prescott⁷,
Kristian Tveten⁷, Thorsten Gerstner⁸, Brianna Pruniski⁹, Stephanie DiTroia¹⁰, Grace E. VanNoy¹⁰,
Heidi L. Rehm¹⁰, Heather McLaughlin¹¹, Hanno J. Bolz^{12,13}, Ulrich Zechner^{12,14}, Emily Bryant¹⁵,
Tiffani McDonough¹⁵, Stefan Kindler³ and Robert Bähring^{1*}

UNCORRECTED MANUSCRIPT

¹ Institute for Cellular and Integrative Physiology, Center for Experimental Medicine, University Hospital Hamburg-Eppendorf, Hamburg, Germany

² Southeast University, Nanjing, China

³ Institute for Human Genetics, University Hospital Hamburg-Eppendorf, Hamburg, Germany

⁴ Department of Neurology and Epileptology, Hertie-Institute for Clinical Brain Research, Tübingen, Germany

⁵ University Center for Rare Diseases, Institute for Human Genetics, University Hospital, Leipzig, Germany

⁶ Department of Clinical Genetics, Leiden University Medical Center, Leiden, The Netherlands

⁷ Department of Medical Genetics, Telemark Hospital Trust, Skien, Norway

⁸ Department of Child Neurology and Rehabilitation and Department of Pediatrics, Hospital of Southern Norway, Arendal, Norway

⁹ Division of Genetics & Metabolism, Phoenix Children's Medical Group, Phoenix, AZ, USA

¹⁰ Center for Mendelian Genomics and Program in Medical and Population Genetics, Broad Institute of MIT and Harvard, Cambridge, MA, USA

¹¹ Invitae Corporation, San Francisco, CA, USA

¹² Senckenberg Centre for Human Genetics, Frankfurt/Main, Germany

¹³ Institute of Human Genetics, University Hospital of Cologne, Cologne, Germany

¹⁴ Institute of Human Genetics, University Medical Center Mainz, Mainz, Germany

¹⁵ Ann & Robert H Lurie Children's Hospital of Chicago, Department of Pediatrics, Northwestern University Feinberg School of Medicine, Chicago, IL, USA

*** To whom correspondence should be addressed at:** Institute for Cellular and Integrative Physiology, Center for Experimental Medicine, University Hospital Hamburg-Eppendorf, Martinistr. 52, 20246 Hamburg, Germany. Tel.: +49+40 7410 5 8638; Fax: +49+40 7410 5 9127; E-mail: r.baehring@uke.de

Abstract

Here, we report on six unrelated individuals, all presenting with early-onset global developmental delay, associated with impaired motor, speech and cognitive development, partly with developmental epileptic encephalopathy and physical dysmorphisms. All individuals carry heterozygous missense variants of *KCND2*, which encodes the voltage-gated potassium (Kv) channel alpha-subunit Kv4.2. The amino acid substitutions associated with the variants, p.(Glu323Lys) (E323K), p.(Pro403Ala) (P403A), p.(Val404Leu) (V404L) and p.(Val404Met) (V404M), affect sites known to be critical for channel gating. To unravel their likely pathogenicity, recombinant mutant channels were studied in the absence and presence of auxiliary beta-subunits under two-electrode voltage-clamp in *Xenopus* oocytes. All channel mutants exhibited slowed and incomplete macroscopic inactivation, and the P403A variant in addition slowed activation. Co-expression of KChIP2 or DPP6 augmented the functional expression of both wild-type and mutant channels, however, the auxiliary beta-subunit-mediated gating modifications differed from wild-type and among mutants. To simulate the putative setting in the affected individuals, heteromeric Kv4.2 channels (wild-type plus mutant) were studied as ternary complexes (containing both KChIP2 and DPP6). In the heteromeric ternary configuration, the E323K variant exhibited only marginal functional alterations compared to homomeric wild-type ternary, compatible with mild loss-of-function. By contrast, the P403A, V404L and V404M variants displayed strong gating impairment in the heteromeric ternary configuration, compatible with loss or gain-of-function. Our results support the etiological involvement of Kv4.2 channel gating impairment in early-onset monogenic global developmental delay. In addition, they suggest that gain-of-function mechanisms associated with a substitution of V404 increase epileptic seizure susceptibility.

Introduction

Global developmental delay (GDD) is defined as a significant delay in two or more developmental domains including (a) gross or fine motor behavior, (b) speech and language, (c) cognition, (d) personal-social skills and (e) activities of daily living, affecting children under the age of 5 (1, 2). With a prevalence of 1 – 3 %, GDD represents one of the most common conditions observed in paediatrics (3-5). GDD is frequently caused by heterozygous *de novo* variants in developmental genes, particularly those expressed in neurons, and thus, often associates with brain malformations and/or altered neuronal functioning (6). The latter may include changes in excitability and discharge behavior, known to be directly controlled by ion channels in neuronal cell membranes, first and foremost voltage-dependent potassium (Kv) channels. The Kv channels are encoded by a large gene superfamily with twelve subfamily members (7; see also Supplementary Material, Fig. S1). The specific role of a particular Kv channel subtype in cellular neurophysiology is determined by its relative expression level and subcellular localization, as well as its voltage dependencies and kinetics of activation and inactivation. Members of the Kv4 subfamily, especially Kv4.2, mediate a subthreshold-activating somatodendritic A-type (i.e., rapidly activating and inactivating) current (I_{SA} ; 8). The Kv4 channel-mediated I_{SA} is involved in many aspects of cellular neurophysiology, including action potential repolarization and frequency-dependent spike broadening (9), control of dendritic excitation and action potential back-propagation (10), as well as synaptic filtering (11) and synaptic plasticity (12). Notably, the Kv4 channel-mediated I_{SA} is down-regulated in animal models of cortical malformations and epilepsy (13-19).

Like all members of the Kv superfamily, Kv4 channel α -subunits consist of six transmembrane segments (S1 - S6), with cytoplasmic N- and C-termini and a re-entrant loop between S5 and S6, which harbors the potassium selectivity filter sequence (Fig. 1A). The α -subunits tetramerize to form functional channels. Within a tetramer, the S1 – S4 helices (particularly the positively charged amino acid residues in S4) function as voltage sensors residing in the channel periphery. The S5 and S6 helices surround the central ion conduction pathway with the intertwined and flexible distal S6 segments functioning as the cytoplasmic gate (20). Mechanical coupling of the voltage sensors to the cytoplasmic

gate, which allows for voltage-dependent channel opening and closing, is provided by mutual interactions between residues in the S4S5 linker and the distal S6 segment (21, 22; Fig. 1). In Kv4 channels these residues are also critically involved in inactivation (23, 24).

Native Kv4 channels are thought to form ternary complexes with auxiliary Kv channel interacting proteins (KChIPs) and/or dipeptidyl-peptidase-related proteins (DPPs; 25). In heterologous expression systems, both KChIPs and DPPs increase Kv4 channel surface expression (26-30). Moreover, both auxiliary β -subunits modulate Kv4 channel gating in a specific manner: KChIPs cause a slowing of macroscopic inactivation and a positive shift in the voltage dependence of steady-state inactivation (26, 27, 29, 31), whereas DPPs cause an acceleration of macroscopic inactivation and a negative shift in the voltage dependencies of both activation and steady-state inactivation (28, 30, 32). Both auxiliary β -subunits accelerate the recovery from inactivation (26-32). These specific modifications have to be taken into account when evaluating Kv4 channel function in a native setting and when considering the likely pathogenicity of mutant variants.

Kv4 channels are encoded by three different genes (*KCND1* – 3; 33); Supplementary Material, Fig. S1). Here, we report on six unrelated individuals with early-onset GDD and heterozygous missense variants of *KCND2*. The associated amino acid substitutions, p.(Glu323Lys) (E323K), p.(Pro403Ala) (P403A, two individuals), p.(Val404Leu) (V404L, two individuals) and p.(Val404Met) (V404M), affect residues, which are involved in controlling the cytoplasmic gate. Functional testing of mutant variants revealed distinct perturbations of channel gating, which are compatible with both a partial loss-of-function (LOF) and gain-of-function (GOF). Our findings strongly implicate Kv4.2 channel gating impairment in the etiology of early-onset GDD, and suggest that substituting V404 increases epileptic seizure susceptibility.

Results

Clinical and genomic data

In this study, we report on six individuals (case 1 - 6) from six unrelated families with diverse ethnic background, all affected by early-onset GDD of distinct severity. In each case, first symptoms were noted within the first six months of life (Table 1 and Supplementary Material, Clinical reports). All six individuals presented with significant delays in motor, speech and cognitive development. Five individuals exhibited muscle hypotonia (case 2 - 6), and three individuals seizures (case 4, 5 and 6). Three individuals showed visual impairments (case 2, 3 and 5), presenting with either progressively declining vision and a strong evidence for rod/cone dystrophy (case 2), cortical visual impairment combined with intermittent lateral nystagmus (case 3) or lack of fixation and strabismus associated with hypomyelination of the visual tract (case 5). Mild physical dysmorphisms were observed for two individuals (case 2 and 6), including either a tall forehead, small mouth, high arched palate, short and small nose, bilateral epicanthal folds and mild two-three toe syndactyly (case 2), or deep set almond shaped eyes, pointed chin, prominent brow ridge, small nose, large anteriorly rotated ears and tall forehead (case 6). Finally, in two individuals brain malformations were detected: Pronounced cortical frontotemporal brain atrophy with mild expansion of inner liquor spaces (case 5), or decrease in both periventricular and deep white matter combined with prominent ventricles (case 6). Noteworthy, in three individuals (case 4, 5 and 6) a developmental epileptic encephalopathy was diagnosed (see Supplementary Material, Clinical reports for electroencephalographical details and pharmacological treatment). One of these individuals (case 5) died at 21 years of age, the cause of death being unknown.

Utilizing next-generation sequencing, we identified different heterozygous missense variants of *KCND2* (NM_012281.3) in the reported individuals. In each case the *KCND2* variant represented the only or most convincingly disease-related gene variant (Supplementary Material, Clinical reports). In four individuals (case 3 - 6) a *de novo* origin of the variant was confirmed. For the remaining two cases (case 1 and 2) the origin of the *KCND2* variant could not be determined owing to the lack of parental DNA specimens. Two individuals (case 2 and 3) carry the same gene variant, and in two other individuals (case 4 and 5) two distinct nucleotide exchanges result in the same amino acid substitution.

Thus, we are dealing with four different amino acid substitutions: c.967G>A;p.(Glu323Lys) (case 1), c.1207C>G;p.(Pro403Ala) (case 2 and 3), c.1210G>T;p.(Val404Leu) (case 4), c.1210G>C;p.(Val404Leu) (case 5) and c.1210G>A;p.(Val404Met) (case 6). Noteworthy, the three individuals diagnosed with developmental epileptic encephalopathy (case 4, 5 and 6) all harbor Val404 substitutions (Table 1). None of the newly identified *KCND2* variants is listed in the public gnomAD database (<https://gnomad.broadinstitute.org/>; gnomAD v2.1.1, GRCh37/hg19). Applied bioinformatics programs predicting the functional relevance of variants (CADD, REVEL, M-CAP, SIFT, Polyphen 2) uniformly predict a deleterious effect on protein function. While the 1210G>A;p.(Val404Met) variant has been previously identified in monozygotic twins affected by severe, intractable seizures and autism (34), the remaining variants are novel. All identified *KCND2* variants affect highly conserved Kv4.2 amino acid residues (Supplementary Material, Fig. S1) critical for channel gating (Fig. 1; 21-23, 35), thus providing initial evidence for their likely pathogenicity. For simplicity, amino acid substitutions and corresponding mutant Kv4.2 channels will be referred to as E323K, P403A, V404L and V404M, respectively.

Functional characterization of mutant Kv4.2 channels in the absence and presence of auxiliary subunits

The four different amino acid substitutions affect sites, which are involved in the operation of the cytoplasmic gate (Fig. 1; 21-23, 35). To assess the hypothesis that all four amino acid substitutions critically influence gating with a detrimental impact on normal channel function, recombinant wild-type (WT) and mutant Kv4.2 channels were expressed alone or together with auxiliary β -subunits in *Xenopus* oocytes and functionally characterized under two-electrode voltage-clamp (see Materials and Methods).

Kv4.2 WT and all tested mutants mediated outward currents in response to depolarizing voltage pulses, albeit with extremely small amplitudes for E323K and P403A. Like Kv4.2 WT, all mutants exhibited increased current amplitudes when co-expressed with either KChIP2 or DPP6, although this effect was

moderate for E323K and especially for P403A (Fig. 2A and B; Supplementary Material, Table S1). Thus, the mutant Kv4.2 proteins are able to form functional channels and interact with both types of auxiliary β -subunits. For V404L and V404M, the voltage dependence of activation was similar to Kv4.2 WT, but E323K and P403A showed an apparent positive shift of ~ 10 and ~ 60 mV, respectively (Fig. 2C; Supplementary Material, Table S1). For both WT and mutant channels, the voltage dependence of activation was steepened by auxiliary β -subunit co-expression with a negative shift caused by DPP6 (Fig. 2C; Supplementary Material, Table S1).

For all tested mutants, the time course of the currents differed from Kv4.2 WT (Fig. 3). Notably, P403A mediated extremely slow activating currents, which did not reach a peak during the applied test pulse, whereas the other mutants showed virtually unaltered activation kinetics. However, the initial current decay kinetics were slowed, and the remaining current at the end of the test pulse was increased for these mutants (Fig. 3; Supplementary Material, Table S2). For P403A, KChIP2 co-expression caused an acceleration of activation kinetics, so that the currents reached a peak during the test pulse, thereby unveiling slow decay kinetics. By contrast, DPP6 did not affect the activation kinetics of P403A, and current decay was only apparent with longer test pulses (Supplementary Material, Fig. S2). The finding that P403A-mediated currents decayed in response to prolonged depolarization, albeit extremely slowly, indicates that, similar to the other mutants, P403A undergoes inactivation. Macroscopic inactivation of the other mutants was modified by KChIP2, but the effects differed from Kv4.2 WT. For E323K, KChIP2 co-expression caused an acceleration rather than a slowing, whereas for both V404L and V404M, KChIP2 co-expression caused an extreme slowing of current decay. DPP6 caused the typical acceleration of current decay for E323K, V404L and V404M (Fig. 3; Supplementary Material, Table S2).

Next, the voltage dependence of steady-state inactivation and the kinetics of recovery from inactivation were studied (Fig. 4). Compared to Kv4.2 WT, the voltage dependence of steady-state inactivation was negatively shifted for E323K and V404M, and for all examined mutants the amount of inactivation at the most depolarized voltage tested was incomplete. KChIP2 caused the typical positive shift in the

voltage dependence of steady-state inactivation for E323K and V404L, but not for V404M, whereas DPP6 caused the typical negative shift for V404L and V404M, but not for E323K (Fig. 4A; Supplementary Material, Table S2). The recovery from inactivation was accelerated compared to Kv4.2 WT for E323K but slowed for V404L and V404M. KChIP2 caused the typical acceleration of recovery kinetics for all of these mutants. Notably, the typical acceleration of recovery kinetics mediated by DPP6 was seen for E323K, whereas the recovery kinetics of V404L and V404M remained virtually unaffected by DPP6 (Fig. 4B; Supplementary Material, Table S2). For P403A, the analysis of the voltage dependence of steady-state inactivation and recovery kinetics was restricted to the data obtained in the presence of auxiliary β -subunits. A comparison of the voltage dependencies of steady-state inactivation for P403A in the presence of KChIP2 or DPP6 with corresponding WT data suggested that the P403A substitution also caused inactivation to be incomplete at the most depolarized voltage tested. Remarkably, the voltage dependence of steady-state inactivation adopted a biphasic shape for P403A + KChIP2, which persisted if KChIP2 was massively overexpressed (data not shown). A comparison of the recovery kinetics obtained for P403A in the presence of KChIP2 or DPP6 with corresponding WT data suggested that the P403A substitution caused a slowing of recovery kinetics (Fig. 4 A and B; Supplementary Material, Table S2).

Heteromeric assembly of wild-type and mutant channel subunits and ternary complex formation

All *KCND2* variants reported herein are monoallelic, compatible with an autosomal dominant mode of inheritance. Thus, we tested whether and how mutant co-expression influences the currents mediated by Kv4.2 WT (Supplementary Material, Fig. S3). For E323K, V404L and V404M the co-expression with WT resulted in currents with intermediate characteristics. Titration effects were particularly obvious for the relative current at the end of the test pulse, albeit with apparently different cRNA dose dependencies for the individual mutants. P403A co-expression at equal cRNA amounts led to an almost complete suppression of the fast macroscopic inactivation of Kv4.2 WT, while a fourfold excess of mutant cRNA gave rise to slowly activating currents with no peak during the applied test pulse (Supplementary Material, Fig. S3, Tables S1 and S2). These results substantially differed from the theoretical sum of currents as predicted for two separate homomeric WT and P403A channel

populations (Supplementary Material, Fig. S3), strongly suggesting WT and mutant Kv4.2 α -subunit co-assembly.

Native Kv4 channels are thought to form ternary complexes with KChIPs and DPPs (25). Therefore, heteromeric (WT + mutant) Kv4.2 channels were simultaneously co-expressed with both KChIP2 and DPP6 to simulate the putative setting in the affected individuals (see Materials and Methods). Properties of WT + mutant ternary channels were compared with those of homomeric WT ternary. Averaged peak current amplitudes were similar for WT ternary, WT + V404L ternary and WT + V404M ternary, whereas WT + E323K ternary and WT + P403A ternary mediated smaller currents (Fig. 5A, B and C; Supplementary Material, Table S1). The voltage dependence of activation was indistinguishable from homomeric WT ternary for WT + E323K ternary, shifted positive for WT + P403A ternary and negative for both WT + V404L ternary and WT + V404M ternary (Fig. 5D; Supplementary Material, Table S1). Studying the inactivation properties of WT + mutant ternary channels revealed that their macroscopic inactivation kinetics diverged to different degrees from homomeric WT ternary. WT + E323K ternary-mediated currents were very similar to those of homomeric WT ternary, except that macroscopic inactivation was not quite complete. However, the other mutants exerted a prominent effect on macroscopic inactivation, even in the heteromeric ternary configuration. Current decay was slowed, and the remaining current at the end of the test pulse was increased. In the heteromeric ternary configuration, the impact of V404L was stronger than that of V404M, and P403A exerted the strongest effect on macroscopic inactivation (Fig. 5E and F; Supplementary Material, Table S2). As a measure of LOF or GOF the combined mutant effects on current amplitude and decay kinetics were quantified by calculating the integral below the respective current traces (Fig. 5G; see Supplementary Material, Table S1 and Discussion). Concerning the voltage dependence of steady-state inactivation, WT + V404L ternary and WT + V404M ternary channels were virtually identical to homomeric WT ternary, whereas WT + E323K ternary and WT + P403A ternary inactivated at slightly more depolarized voltages (not significant for WT + E323K ternary), and steady-state inactivation was incomplete for WT + P403A ternary (Fig. 5H). The kinetics of recovery from inactivation resembled homomeric WT

ternary for WT + E323K ternary and WT + V404M ternary, whereas WT + P403A ternary and WT + V404L ternary recovered from inactivation more slowly (Fig. 5I; Supplementary Material, Table S2).

Ternary Kv4.2 channel analysis was extended to the kinetics of activation and deactivation (Fig. 6). The slow activation kinetics caused by the P403A substitution (see Fig. 3A) were still apparent in the heteromeric ternary configuration and correlated with the positively shifted voltage dependence of activation for WT + P403A ternary (see Fig. 5D). The other variants did not significantly influence activation kinetics in the heteromeric ternary configuration (Fig. 6A and B; Supplementary Material, Table S1). Finally, the kinetics of channel closure were examined. Remarkably, all heteromeric WT + mutant ternary channels showed slower deactivation kinetics than homomeric WT ternary. The effect was moderate for WT + E323K ternary, stronger for WT + V404M ternary, and most prominent for WT + V404L ternary and WT + P403A ternary (Fig. 6C and D; Supplementary Material, Table S1). Taken together, these data show that in the heteromeric ternary configuration some forms of gating impairment become less apparent, while others persist. The latter are compatible with both LOF and GOF. The positively shifted voltage dependence and slow kinetics of activation caused by P403A (partial LOF) and the extremely slow macroscopic inactivation and deactivation kinetics caused by both P403A and V404L (GOF) should be especially noted in this context (Supplementary Material, Tables S1 and S2).

Kv4.2 channels inactivate more readily from pre-open closed states than from the open state (36). Since this preferential closed-state inactivation (CSI) plays an important role in dendritic excitation and synaptic plasticity, and since the amino acid substitutions identified herein affect sites, which are critically involved in gating, we examined whether CSI is still the predominant inactivation pathway in the heteromeric WT + mutant ternary channels. To that end, we tested for kinetic features of inactivation indicative of a significant contribution of open-state inactivation (Supplementary Material, Fig. S4). However, we neither found an obvious decline of inactivation time constants with increasing depolarization (Supplementary Material, Fig. S4A), nor did the rate of inactivation match open probability during moderate depolarization (Supplementary Material, Fig. S4B). Based on these tests,

which supported the presence of preferential CSI in both homomeric WT ternary and heteromeric WT + mutant ternary channels, we finally determined the kinetics of CSI at a voltage of -60 mV, expected to induce negligible open probability. We found that CSI on- and off-rates were specifically modified in all WT + mutant ternary channels, except for WT + E323K ternary (Supplementary Material, Fig. S4C). The structure-function relationship of the mutant impact on Kv4.2 channel CSI, the putative pathogenic effects of Kv4.2 channel LOF and GOF and the clinical phenotypes associated with Kv4 channel dysfunction will be discussed.

UNCORRECTED MANUSCRIPT

Discussion

We have studied recombinant mutant Kv4.2 channels with single amino acid substitutions, corresponding to heterozygous *KCND2* missense variants found in a cohort of infants presenting with GDD. The occurrence of two identical and two similar *KCND2* variants, and the independent recurrence of a previously reported variant (34) within our study, identify the respective codons as putative disease-associated mutational “hotspots”. Combined with our functional data this corroborates the particular importance of the S4S5 linker and the distal S6 segment for accurate Kv4.2 channel function. By testing the mutant Kv4.2 channels in a native setting, we provide strong evidence that the identified *KCND2* variants lead to a syndromic neurodevelopmental disorder, which includes impaired motor development, speech and cognition, as well as possible epileptic seizures, brain malformations and physical dysmorphisms.

Mutation-associated impairment of channel gating

All *KCND2* variants reported herein affect Kv4.2 amino acid residues in highly conserved domains, which are directly involved in operating the cytoplasmic gate. Therefore each of the four amino acid substitutions examined, E323K, P403A, V404L and V404M, in itself profoundly alters Kv4.2 channel gating. P403, which is altered in case 2 and 3 (Table 1), represents the second proline of a PXP motif, highly conserved in Kv1 - Kv4 channels (see Supplementary Material, Fig. S1). Our study demonstrates a strong positive shift in the voltage dependence of activation and extremely slow activation kinetics for P403A. These findings support the general idea that the PXP motif allows the S6 helix to bend, which is critical for opening and closing of the cytoplasmic gate (20). Moreover, our data obtained in the presence of auxiliary β -subunits suggest that the P403A substitution *per se* attenuates Kv4.2 channel inactivation, supporting the notion that S6 motion is involved in Kv4.2 channel inactivation (23).

Intriguingly, substituting the valine residue directly following the PXP motif (V404L in case 4 and 5, and V404M in case 6) leaves activation kinetics more or less unaffected, but critically influences Kv4.2 channel inactivation. In V404L and V404M inactivation is attenuated at depolarized voltages. In fact, both mutants show a biphasic voltage dependence of inactivation with typical U-type features (i.e.,

inactivation is strongest at intermediate voltages), which is a most obvious indicator of preferential CSI (36). Notably, this feature is not evident in Kv4.2 WT, because these channels normally accumulate in closed-inactivated states at all relevant membrane voltages (23, 36). Yet, U-type features have been described previously for certain Kv4.2 mutants including V404M (23, 35). The U-type features observed herein for both V404L and V404M can be explained by a strong impairment of inactivation once these channels have opened, presumably due to their slowed channel closure, as suggested previously for V404M (35; see also Fig. 6) and for a similar mutant of Kv4.1 (24). It is widely accepted that Kv4 channels need to close in order to fully inactivate (36), however, the actual mechanism of Kv4 channel CSI is still unknown. It has been proposed that the S4S5 linker and the distal S6 segment may lose their mutual physical contact during Kv4 channel CSI (23). This view is challenged by the finding that, despite the larger side chain volume of methionine (168 \AA^3) compared to valine (139 \AA^3 ; Fig. 1C; 37), which may actually favor physical contact, CSI is enhanced (i.e., the voltage dependence of inactivation is negatively shifted) for V404M (35; see also Fig. 4A). However, it should be noted that a previously studied V404A mutant with a reduced side chain volume of 90 \AA^3 also displayed a negative shift in the voltage dependence of inactivation (23), even larger than that observed for V404M in the present study. Moreover, our results show that, despite the similar side chain volumes of methionine (168 \AA^3) and leucine (165 \AA^3 ; Fig. 1C; 37) the effects of V404M and V404L are distinct. Intriguingly, in one of our individuals (case 1) E323, a critical thermodynamic coupling partner of V404 (23, 38), is affected. In the E323K mutant, not only side chain volume, which is increased from 141 to 170 \AA^3 (Fig. 1C; 37), but also the charge of the side chain (from negative to positive) is modified. As a consequence of the E323K substitution the voltage dependence of inactivation becomes more negative but shallow, and inactivation is incomplete at depolarized voltages. It is remarkable that reducing the volume (from 141 to 90 \AA^3) and neutralizing the charge of the side chain at this position (E323A) also caused a negative shift (23), whereas a highly conservative amino acid substitution (E323D) apparently caused a positive shift in the voltage dependence of inactivation (35). Taken together, these findings suggest that, in addition to side chain volume and charge, other structural features critically determine Kv4.2 channel CSI. Also, in addition to E323 and V404 other amino acid residues, located outside the mutational "hotspots" identified herein (38), may be involved in the dynamic coupling between the

S4S5 linker and the distal S6 segment during the process of Kv4.2 channel CSI. Obviously, the structure-function relationship of Kv4.2 channel CSI, although already studied in some detail (35, 36, 38, 39), has not been resolved with sufficient clarity and requires further examination in a different context. Of central importance for the present study, although none of the mutations leads to a loss of CSI in the heteromeric WT + mutant ternary configuration, each of them specifically modifies CSI on- and off-rates of the channel complex (Supplementary Material, Fig. S4).

LOF and GOF in a native setting

Native Kv4 channels form complexes with auxiliary KChIPs and DPPs, both known to enhance channel surface expression and to specifically modify channel gating (26, 28). In fact, Kv4 channels in many neurons are likely to be ternary complexes containing both types of auxiliary β -subunits (25). Thus, apparently low expression levels and/or conspicuous gating properties observed for a channel mutant, if examined in isolation, may be pushed into the background if auxiliary β -subunits are present, provided the mutation itself does not affect the interaction. Here, we chose KChIP2 and DPP6 splice-variants abundantly expressed in the hippocampus (30, 42, 43) for auxiliary β -subunit co-expression. Our finding that for both Kv4.2 WT and all tested mutants, β -subunit co-expression causes a significant increase in peak current amplitude suggests that the mutants are still able to interact with auxiliary β -subunits, although in some cases the effects of the β -subunits on channel gating are absent or differ from those observed for Kv4.2 WT. These special mutant features were not further examined in the present study.

Instead, the Kv4.2 mutants were tested in a heteromeric ternary configuration (see Fig. 5 and 6), to judge the likely pathogenicity of the corresponding heterozygous *KCND2* variants in our cohort of individuals. The significantly reduced peak current amplitudes found for WT + E323K ternary and WT + P403A may be classified as partial LOF, however, the current amplitudes measured in a heterologous expression system must be interpreted with caution, and immunocytochemical analysis suggested equal amounts of membrane protein for WT ternary, WT + E323K ternary and WT + P403A ternary (data not shown). For WT + E323K ternary all other modifications (tentatively GOF; see

Supplementary Material, Tables S1 and S2) failed to reach significance. WT + P403A ternary shows further signs of partial LOF: the persistently slowed kinetics and positively shifted voltage dependence of activation and the slowed recovery kinetics. However, WT + P403A ternary also exhibits GOF features, namely slowed and incomplete macroscopic inactivation combined with slowed deactivation and a positively shifted voltage dependence of inactivation. Similarly, WT + V404L ternary exhibits both partial LOF (steepened voltage dependence of inactivation and slowed recovery kinetics) and GOF features (slowed and incomplete macroscopic inactivation combined with slowed deactivation and negatively shifted as well as steepened voltage dependence of activation), whereas V404M exhibits only GOF features (incomplete macroscopic inactivation combined with slowed deactivation and negatively shifted voltage dependence of activation) in the heteromeric ternary configuration (see also Supplementary Material, Tables S1 and S2).

The crucial question to be asked is whether and how the LOF and GOF features observed for the individual mutants in a native setting may influence cellular neurophysiology and/or neurodevelopmental aspects. Certainly, the most striking LOF feature observed in our study is the persistently impaired activation of WT + P403A ternary, which is very likely to suppress I_{SA} . The I_{SA} suppression is expected to compromise the control of dendritic excitation, including facilitated generation and back-propagation of action potentials, constitutive frequency-independent spike-broadening and reduced dampening of excitatory postsynaptic potentials (9-12; possibly in case 1, 2 and 3). The most striking GOF feature, observed equally for WT + P403A ternary, WT + V404L ternary and WT + V404M ternary in our study, albeit with quantitative differences, is the slowed and/or incomplete current relaxation at all voltages, presumably caused by slowed channel closure. In affected neurons this feature is expected to cause an increase in potassium conductance and, thus, hyperpolarization of the resting membrane potential for tens to hundreds of milliseconds following one or more action potentials. Due to putatively very slow I_{SA} activation kinetics, P403A expressing neurons may show this behavior only following an extended spike train (possibly in case 2 and 3), whereas in V404L and V404M expressing neurons a single spike may be sufficient to cause an unphysiological pause in electrical activity (possibly in case 4, 5 and 6). Thus, due to the fast activation and extremely

slow deactivation kinetics of WT + V404L ternary, V404L expressing neurons (case 4 and 5) might be most prominently affected.

Potassium channel dysfunction of genetic origin may cause epilepsy and neurodevelopmental disorders including autism (7, 44). The disease-related Kv channel gene families (and affected types of α -subunit) include *KCNA* (Kv1), *KCNB* (Kv2), *KCNC* (Kv3), *KCND* (Kv4), *KCNQ* (Kv7), *KCNV* (Kv8) and *KCNH* (Kv10; (7); see also Supplementary Material, Fig. S1). Although the majority of pathogenic Kv channel gene variants causing neurological disorders associated with epilepsy exhibits LOF, we currently see a growing number of GOF variants associated with epilepsy; i.e., enhanced intrinsic Kv channel activity may lead to network hyperexcitability (45). This seemingly paradoxical finding may be explained by one or more of the following pathogenic mechanisms: (1) Kv channel GOF and reduced intrinsic excitability in inhibitory interneurons may lead to hyperexcitability in postsynaptic neurons (disinhibition); (2) Kv channel GOF and a resultant strong (after-) hyperpolarization following an action potential may particularly well remove sodium channel inactivation, thereby leading to facilitated action potential firing; (3) Kv channel GOF leading to reduced activity of a neuron may increase the number of synapses and/or the number of postsynaptic glutamate receptors (homeostatic plasticity; 45). The mechanism of disinhibition has been suggested as an explanation for the occurrence of epileptic seizures in the reported twin boys carrying the V404M variant (34) and may thus also apply to case 4, 5 and 6 of the present study, in which epileptic seizures were observed (see Table 1). More recently, membrane hyperpolarization and reduced excitability due to potassium channel GOF have been linked to developmental disorders associated for instance with impaired cell migration, which may eventually lead to neuroanatomical abnormalities and neurodevelopmental disorders as well as numerous non-neuronal dysmorphic physical features (46). Although the *KCND* (Kv4) subfamily of Kv channel genes has thus far received little attention in this context, the latter mechanism may explain how Kv4.2 channel GOF due to the *KCND2* variants described herein can lead to multi-domain GDD (case 1 - 6; see Table 1).

***KCND2* variants and clinical phenotypes**

The first *KCND2* variant associated with a neurological phenotype was a paternally-inherited deletion found in a female with refractory temporal lobe epilepsy starting at the age of 13 years, with no histological abnormalities, but cognitive impairment preceding her history of epilepsy (47). In that individual, a 5 bp deletion leads to a frameshift and a premature stop codon, and the resultant mutant Kv4.2 protein is predicted to lack the last 44 amino acids (N587fsX1). The observed partial LOF may be attributed to the loss of multiple extracellular signal receptor kinase (ERK) phosphorylation sites (48) and the loss of interaction motifs for the cytoskeletal proteins filamin (49) and post-synaptic density 95 (PSD-95; 50), both located within this C-terminal region (47). Thus, there is neither genetic nor mechanistic overlap of the N587fsX1 individual with our cohort. Since that individual shows cognitive impairment and did not show epileptic seizures under the age of 13 years, a phenotypic overlap with our cohort at a later stage cannot be excluded, however, she did apparently not show GDD (47). The same may apply to a reported *KCND1* nonsense variant associated with a similar C-terminal truncation detected in a male with epilepsy onset at the age of 8 years and normal intellectual development (51).

More recently a heterozygous *KCND2* missense variant has been identified, which is genetically identical to the variant identified in case 6 of our study (V404M). It was discovered in monozygotic twin boys presenting with early-onset (at the age of two months) intractable seizures, autism, language disability and an overall cognitive functioning in the very low range (34). Similarly, early disease onset, and delayed speech and cognitive development are common phenotypic features in the cohort of individuals described herein (see Table 1). Moreover, within our cohort all three cases with *KCND2* variants affecting V404 (V404L in case 4 and 5 and V404M in case 6) exhibit severe epilepsy, while this phenotype has not been noted in the other three individuals (case 1, 2 and 3, see Table 1). Notably, in case 4, 5 and 6 the *KCND2* variants are associated with net GOF, whereas in case 1, 2 and 3 both LOF and GOF features can be found (see Supplementary Material, Table S1 and S2). Our results suggest that *KCND2* (Kv4.2) GOF rather than LOF variants, associated with the identified mutational "hotspots" (S4S5 linker and distal S6), favor epileptic seizure susceptibility.

In our study, autism was only observed in case 4 (V404L), but not for the other five cases, including the one carrying the previously published V404M variant (34; see Table 1, case 6). Just like the autistic identical twin boys harboring the V404M variant (34) our V404L individual with autism (case 4) is male, whereas our V404M individual (case 6) is female. The absence of autism in case 6 may reflect the generally found lower probability for females to be diagnosed with autism (52). Notably, the identical twins with autism harboring the V404M variant also share variants of other genes besides *KCND2*, including *BICCI* (coding for an RNA binding protein), *GPR124* (coding for a G-protein-coupled receptor) and *SLC8A2* (coding for a sodium/calcium exchanger; 34). Thus, autism may not represent a key phenotypic feature associated with *KCND2* variants. On the other hand, our data suggest that delayed motor development and muscle hypotonia are key features of *KCND2* missense variants (see Table 1), although these features were not reported for the identical twins harbouring the V404M variant (34). Apparently, the clinical phenotypes associated with heterozygous *KCND2* missense variants are highly variable. Which of the different phenotypic features (GDD, autism or epileptic seizures) is dominant may depend on the relative proportion of LOF and GOF mutational effects. Moreover, additional gene variants and other factors, including sex (52), may modify *KCND2*-associated phenotypes.

Pharmacological interventions in developmental epileptic encephalopathy are usually based on inhibition of excitatory ligand and voltage-dependent ion channels, inhibition of excitatory neurotransmitter release and/or potentiation of GABAergic effects, as evident from the medications applied in case 4, 5 and 6 of our cohort (53; see also Supplementary Material, Clinical reports). Based on the knowledge gained from the genetic and biophysical analyses performed in the present study, a more specific and presymptomatic pharmacological intervention, possibly one which directly targets Kv4.2 channels in an appropriate manner, would be desirable. In particular, considering neurodevelopmental disorders associated with *KCND2* (Kv4.2) GOF, Kv4.2 channel inhibition in early childhood may be an option to be considered. Pharmacological compounds with intriguing properties, including toxins isolated from various tarantula (54, 55) and scorpion venoms (56, 57), may serve as

lead structures. The tarantula toxins inhibit Kv4 channels by gating modification including a positive shift in the activation curve (54, 55), a feature that may target predominantly the subthreshold active neuronal I_{SA} rather than cardiac I_{to} . The scorpion toxins selectively inhibit Kv4 channels with DPPs bound (56), a combination found predominantly in the brain. These compounds and newly developed ones should be explored in more detail to address their effectivity in neuronal and their tolerability in cardiac tissue. It would be desirable if they may eventually allow for early mechanism-based precision medicine to benefit young individuals and minimize developmental disturbances.

UNCORRECTED MANUSCRIPT

Materials and Methods

Individuals and genomic analysis

Research subjects. Written informed consent for all subjects was obtained in accordance with protocols approved by the respective ethics committees of the institutions involved in this study.

Genetic analysis. Some of the investigators presenting affected individuals in this study were connected through GeneMatcher, a web-based tool for researchers and clinicians working on identical genes (58). The different centers involved in this study utilized comparable protocols for DNA isolation, whole-exome and -genome sequencing, bioinformatics processing and variant interpretation. For case 2 and 4 sequencing and data analysis was performed by the Genomics Platform at the Broad Institute of MIT and Harvard and the Senckenberg Centre for Human Genetics, respectively. The *KCND2* variant of case 6 was identified via targeted-gene panel analysis.

Structural modeling

Structural homology modeling based on the crystal structure coordinates of a Kv1.2-Kv2.1 chimera (PDB accession number 2R9R; 59) was performed with PyMol (Schrödinger). Amino acid substitutions were simulated considering the most likely backbone-dependent rotamer orientation, and the putative steric consequences of the amino acid substitution within a distance of 8 Å were taken into account.

Plasmids and *in vitro* transcription

KCND2 variants were inserted into a pGEM-HE vector containing the complete coding region of the human Kv4.2 cDNA (60) utilizing the Q5® Site-Directed Mutagenesis Kit (New England Biolabs) and verified by Sanger sequencing. For auxiliary β -subunit co-expression we used the human KChIP2b splice variant (previously referred to as KChIP2.1; 27) in pGEM-HE and the human DPP6s splice variant (also referred to as DPPX-S; 61); gift from Henry Jerng, Baylor College of Medicine, Houston, TX) in a pUC-derivative. Transformed JM109 *E.coli* cells (Promeda) were grown in Luria Broth medium complemented with ampicillin, and plasmids were isolated using the QIAprep Spin Miniprep

Kit (QIAGEN). Purified plasmids were linearized using NotI (New England Biolabs), and the RiboMaxLargeScale RNA production system T7 (Promega) was utilized to *in-vitro* transcribe cRNAs.

Heterologous channel expression

Kv4.2 channels were expressed in *Xenopus laevis* oocytes as described previously (23, 38). To express homomeric Kv4.2 channels, 5 ng total cRNA were injected per oocyte. For heteromeric channel expression Kv4.2 WT and mutant cRNAs were injected at a ratio of either 1:1 (2.5 + 2.5 ng per oocyte) or 1:4 (1 + 4 ng per oocyte). Both Kv4.2 WT and mutant homomers were co-expressed with KChIP2 (5 ng cRNA per oocyte) or DPP6 (5 ng cRNA per oocyte). Furthermore, Kv4.2 WT homomers (5 ng cRNA per oocyte) and Kv4.2 WT + mutant heteromers (2.5 + 2.5 ng cRNA per oocyte) were co-expressed with both KChIP2 and DPP6 (both 5 ng cRNA per oocyte) for ternary complex formation. Oocytes were used for electrophysiological recordings one to three days after cRNA injection

Recording techniques and pulse protocols

Currents were recorded at room temperature (20 – 22 °C) under two-electrode voltage-clamp as described previously (23, 38) using TurboTec amplifiers (npi) controlled by PatchMaster software (HEKA). To minimize contamination of small-sized Kv4.2-mediated outward currents at depolarized membrane potentials by endogenous chloride currents we used a low chloride (15 mM) bath solution in most experiments containing (in mM) 7.4 NaCl, 88.6 Na-aspartate, 2 KCl, 1.8 CaCl₂, 1 MgCl₂ and 5 HEPES, pH 7.4 with NaOH. For oocytes expressing ternary complexes the same solution was used with Na-aspartate replaced by NaCl. Pulse protocols are explained in the figure legends. Capacitive current transients were not compensated, and the current measured at -95 mV (approximate E_{rev} for K⁺) was used to calculate the leak current at any other voltage. For the study of activation kinetics of ternary complexes a p/5 protocol was used for leak subtraction.

Data analysis

Data were analysed using FitMaster (HEKA) and Kaleidagraph (Synergy Software). The voltage dependence of activation was analysed based on cord conductances (calculated with $E_{rev} = -95$ mV) and

a 4th order Boltzmann-function as described previously (23, 38). Macroscopic activation kinetics were described by the 10-90% rise time (Supplementary Material, Fig. S2), and macroscopic inactivation kinetics were approximated by a double-exponential function. In addition, the remaining current at the end of a 2.5 s test pulse relative to peak was determined. Deactivating tail current kinetics (at -60 mV) were approximated by a single-exponential function. The voltage dependence of steady-state inactivation was analysed based on a single or, if necessary, the sum of two Boltzmann-functions. Recovery from inactivation (at -100 mV) was described by a single- or, if necessary, a double-exponential function. The biphasic nature of the voltage dependence of steady-state inactivation and recovery kinetics observed for some channels were not further studied, and the analysis was restricted to the more negative and the faster components, respectively. Pooled data are presented as mean \pm SEM, and individual data points are shown for summary bar graphs. Statistical analyses for multiple groups are based on one-way analysis of variance (ANOVA) with Dunnett's post hoc testing, and for two groups on Student's t-test. Data and statistical analysis results are summarized in Supplementary Material, Tables S1 and S2.

Supplementary Material

Clinical reports; Figures S1, S2, S3 and S4 including legends; Supplementary Methods; Tables S1 and S2.

Acknowledgements

We thank the family members for their participation and collaboration. This study makes use of data generated by the DECIPHER community (62). A full list of centers that contributed to the generation of the data is available from <http://decipher.sanger.ac.uk> and via email from decipher@sanger.ac.uk. We thank Telse Kock and Jessica Wollberg for the cloning of Kv4.2 mutant constructs. This work was supported by the Deutsche Forschungsgemeinschaft [BA2055/1-3 and BA2055/6-1 to R.B., HE8155/1-1 to U.B.S.H., LE1030/16-1 to H.L.]; and the China Scholarship Council [201806090432]. H.M. is an employee and shareholder at Invitae Corporation. Sequencing and analysis (case 2) were provided by the Broad Institute of MIT and Harvard Center for Mendelian Genomics (Broad CMG) and was funded by the National Human Genome Research Institute, the National Eye Institute, and the National Heart, Lung and Blood Institute grants [UM1 HG008900, R01 HG009141] and by the Chan Zuckerberg Initiative to the Rare Genomes Project. Funding for the DECIPHER project was provided by the Wellcome Trust.

Conflict of Interest Statement. None declared.

References

1. Shevell, M. (2008) Global developmental delay and mental retardation or intellectual disability: conceptualization, evaluation, and etiology. *Pediatr. Clin. North Am.*, **55**, 1071-1084.
2. Shevell, M., Ashwal, S., Donley, D., Flint, J., Gingold, M., Hirtz, D., Majnemer, A., Noetzel, M., Sheth, R.D. (2003) Practice parameter: evaluation of the child with global developmental delay: report of the Quality Standards Subcommittee of the American Academy of Neurology and The Practice Committee of the Child Neurology Society. *Neurology*, **60**, 367-380.
3. Mithyantha, R., Kneen, R., McCann, E. and Gladstone, M. (2017) Current evidence-based recommendations on investigating children with global developmental delay. *Arch. Dis. Child*, **102**, 1071-1076.
4. Vasudevan, P. and Suri, M. (2017) A clinical approach to developmental delay and intellectual disability. *Clin. Med.*, **17**, 558-561.
5. Srour, M. and Shevell, M. (2014) Genetics and the investigation of developmental delay/intellectual disability. *Arch. Dis. Child*, **99**, 386-389.
6. Deciphering Developmental Disorders, S. (2017) Prevalence and architecture of de novo mutations in developmental disorders. *Nature*, **542**, 433-438.
7. Allen, N.M., Weckhuysen, S., Gorman, K., King, M.D. and Lerche, H. (2020) Genetic potassium channel-associated epilepsies: Clinical review of the Kv family. *Eur. J. Paediatr. Neurol.*, **24**, 105-116.
8. Serodio, P., Kentros, C. and Rudy, B. (1994) Identification of molecular components of A-type channels activating at subthreshold potentials. *J. Neurophysiol.*, **72**, 1516-1529.
9. Kim, J., Wei, D.S. and Hoffman, D.A. (2005) Kv4 potassium channel subunits control action potential repolarization and frequency-dependent broadening in rat hippocampal CA1 pyramidal neurones. *J. Physiol.*, **569**, 41-57.
10. Hoffman, D.A., Magee, J.C., Colbert, C.M. and Johnston, D. (1997) K⁺ channel regulation of signal propagation in dendrites of hippocampal pyramidal neurons. *Nature*, **387**, 869-875.

11. Ramakers, G.M. and Storm, J.F. (2002) A postsynaptic transient K⁺ current modulated by arachidonic acid regulates synaptic integration and threshold for LTP induction in hippocampal pyramidal cells. *Proc. Natl. Acad. Sci. U. S. A.*, **99**, 10144-10149.
12. Watanabe, S., Hoffman, D.A., Migliore, M. and Johnston, D. (2002) Dendritic K⁺ channels contribute to spike-timing dependent long-term potentiation in hippocampal pyramidal neurons. *Proc. Natl. Acad. Sci. U. S. A.*, **99**, 8366-8371.
13. Bernard, C., Anderson, A., Becker, A., Poolos, N.P., Beck, H. and Johnston, D. (2004) Acquired dendritic channelopathy in temporal lobe epilepsy. *Science*, **305**, 532-535.
14. Castro, P.A., Cooper, E.C., Lowenstein, D.H. and Baraban, S.C. (2001) Hippocampal heterotopia lack functional Kv4.2 potassium channels in the methylazoxymethanol model of cortical malformations and epilepsy. *J. Neurosci.*, **21**, 6626-6634.
15. Francis, J., Jugloff, D.G., Mingo, N.S., Wallace, M.C., Jones, O.T., Burnham, W.M. and Eubanks, J.H. (1997) Kainic acid-induced generalized seizures alter the regional hippocampal expression of the rat Kv4.2 potassium channel gene. *Neurosci. Lett.*, **232**, 91-94.
16. Lugo, J.N., Barnwell, L.F., Ren, Y., Lee, W.L., Johnston, L.D., Kim, R., Hrachovy, R.A., Sweatt, J.D. and Anderson, A.E. (2008) Altered phosphorylation and localization of the A-type channel, Kv4.2 in status epilepticus. *J. Neurochem.*, **106**, 1929-1940.
17. Monaghan, M.M., Menegola, M., Vacher, H., Rhodes, K.J. and Trimmer, J.S. (2008) Altered expression and localization of hippocampal A-type potassium channel subunits in the pilocarpine-induced model of temporal lobe epilepsy. *Neuroscience*, **156**, 550-562.
18. Su, T., Cong, W.D., Long, Y.S., Luo, A.H., Sun, W.W., Deng, W.Y. and Liao, W.P. (2008) Altered expression of voltage-gated potassium channel 4.2 and voltage-gated potassium channel 4-interacting protein, and changes in intracellular calcium levels following lithium-pilocarpine-induced status epilepticus. *Neuroscience*, **157**, 566-576.
19. Tsaur, M.L., Sheng, M., Lowenstein, D.H., Jan, Y.N. and Jan, L.Y. (1992) Differential expression of K⁺ channel mRNAs in the rat brain and down-regulation in the hippocampus following seizures. *Neuron*, **8**, 1055-1067.

20. Swartz, K.J. (2004) Towards a structural view of gating in potassium channels. *Nat. Rev. Neurosci.*, **5**, 905-916.
21. Lu, Z., Klem, A.M. and Ramu, Y. (2002) Coupling between voltage sensors and activation gate in voltage-gated K⁺ channels. *J. Gen. Physiol.*, **120**, 663-676.
22. Yifrach, O. and MacKinnon, R. (2002) Energetics of pore opening in a voltage-gated K⁺ channel. *Cell*, **111**, 231-239.
23. Barghaan, J. and Bähring, R. (2009) Dynamic coupling of voltage sensor and gate involved in closed-state inactivation of Kv4.2 channels. *J. Gen. Physiol.*, **133**, 205-224.
24. Jerng, H.H., Shahidullah, M. and Covarrubias, M. (1999) Inactivation gating of Kv4 potassium channels: molecular interactions involving the inner vestibule of the pore. *J. Gen. Physiol.*, **113**, 641-660.
25. Maffie, J. and Rudy, B. (2008) Weighing the evidence for a ternary protein complex mediating A-type K⁺ currents in neurons. *J. Physiol.*, **586**, 5609-5623.
26. An, W.F., Bowlby, M.R., Betty, M., Cao, J., Ling, H.P., Mendoza, G., Hinson, J.W., Mattsson, K.I., Strassle, B.W., Trimmer, J.S. *et al.* (2000) Modulation of A-type potassium channels by a family of calcium sensors. *Nature*, **403**, 553-556.
27. Bähring, R., Dannenberg, J., Peters, H.C., Leicher, T., Pongs, O. and Isbrandt, D. (2001) Conserved Kv4 N-terminal domain critical for effects of Kv channel-interacting protein 2.2 on channel expression and gating. *J. Biol. Chem.*, **276**, 23888-23894.
28. Nadal, M.S., Ozaita, A., Amarillo, Y., de Miera, E.V., Ma, Y., Mo, W., Goldberg, E.M., Misumi, Y., Ikehara, Y., Neubert, T.A. *et al.* (2003) The CD26-related dipeptidyl aminopeptidase-like protein DPPX is a critical component of neuronal A-type K⁺ channels. *Neuron*, **37**, 449-461.
29. Shibata, R., Misonou, H., Campomanes, C.R., Anderson, A.E., Schrader, L.A., Doliveira, L.C., Carroll, K.I., Sweatt, J.D., Rhodes, K.J. and Trimmer, J.S. (2003) A fundamental role for KChIPs in determining the molecular properties and trafficking of Kv4.2 potassium channels. *J. Biol. Chem.*, **278**, 36445-36454.

30. Zagha, E., Ozaita, A., Chang, S.Y., Nadal, M.S., Lin, U., Saganich, M.J., McCormack, T., Akinsanya, K.O., Qi, S.Y. and Rudy, B. (2005) DPP10 modulates Kv4-mediated A-type potassium channels. *J. Biol. Chem.*, **280**, 18853-18861.
31. Beck, E.J., Bowlby, M., An, W.F., Rhodes, K.J. and Covarrubias, M. (2002) Remodelling inactivation gating of Kv4 channels by KCHIP1, a small-molecular-weight calcium-binding protein. *J. Physiol.*, **538**, 691-706.
32. Jerng, H.H., Qian, Y. and Pfaffinger, P.J. (2004) Modulation of Kv4.2 channel expression and gating by dipeptidyl peptidase 10 (DPP10). *Biophys. J.*, **87**, 2380-2396.
33. Isbrandt, D., Leicher, T., Waldschütz, R., Zhu, X., Luhmann, U., Michel, U., Sauter, K. and Pongs, O. (2000) Gene structures and expression profiles of three human *KCND* (Kv4) potassium channels mediating A-type currents I_{TO} and I_{SA} . *Genomics*, **64**, 144-154.
34. Lee, H., Lin, M.C., Kornblum, H.I., Papazian, D.M. and Nelson, S.F. (2014) Exome sequencing identifies de novo gain of function missense mutation in *KCND2* in identical twins with autism and seizures that slows potassium channel inactivation. *Hum. Mol. Genet.*, **23**, 3481-3489.
35. Lin, M.A., Cannon, S.C. and Papazian, D.M. (2018) Kv4.2 autism and epilepsy mutation enhances inactivation of closed channels but impairs access to inactivated state after opening. *Proc. Natl. Acad. Sci. U. S. A.*, **115**, E3559-E3568.
36. Bähring, R. and Covarrubias, M. (2011) Mechanisms of closed-state inactivation in voltage-gated ion channels. *J. Physiol.*, **589**, 461-479.
37. Harpaz, Y., Gerstein, M. and Chothia, C. (1994) Volume changes on protein folding. *Structure*, **2**, 641-649.
38. Wollberg, J. and Bähring, R. (2016) Intra- and intersubunit dynamic binding in Kv4.2 channel closed-state inactivation. *Biophys. J.*, **110**, 157-175.
39. Bähring, R., Barghaan, J., Westermeier, R. and Wollberg, J. (2012) Voltage sensor inactivation in potassium channels. *Front. Pharmacol.*, **3**, 1-8.

40. Amarillo, Y., De Santiago-Castillo, J.A., Dougherty, K., Maffie, J., Kwon, E., Covarrubias, M. and Rudy, B. (2008) Ternary Kv4.2 channels recapitulate voltage-dependent inactivation kinetics of A-type K⁺ channels in cerebellar granule neurons. *J. Physiol.*, **586**, 2093-2106.
41. Jerng, H.H., Kunjilwar, K. and Pfaffinger, P.J. (2005) Multiprotein assembly of Kv4.2, KChIP3 and DPP10 produces ternary channel complexes with I_{SA}-like properties. *J. Physiol.*, **568**, 767-788.
42. Nadal, M.S., Amarillo, Y., de Miera, E.V. and Rudy, B. (2006) Differential characterization of three alternative spliced isoforms of DPPX. *Brain Res.*, **1094**, 1-12.
43. Rhodes, K.J., Carroll, K.I., Sung, M.A., Doliveira, L.C., Monaghan, M.M., Burke, S.L., Strassle, B.W., Buchwalder, L., Menegola, M., Cao, J. *et al.* (2004) KChIPs and Kv4 α subunits as integral components of A-type potassium channels in mammalian brain. *J. Neurosci.*, **24**, 7903-7915.
44. Guglielmi, L., Servettini, I., Caramia, M., Catacuzzeno, L., Franciolini, F., D'Adamo, M.C. and Pessia, M. (2015) Update on the implication of potassium channels in autism: K⁺ channel autism spectrum disorder. *Front. Cell. Neurosci.*, **9**, 1-14.
45. Niday, Z. and Tzingounis, A.V. (2018) Potassium channel gain of function in epilepsy: An unresolved paradox. *Neuroscientist*, **24**, 368-380.
46. Hamilton, M.J. and Suri, M. (2020) "Electrifying dysmorphology": Potassium channelopathies causing dysmorphic syndromes. *Adv. Genet.*, **105**, 137-174.
47. Singh, B., Ogiwara, I., Kaneda, M., Tokonami, N., Mazaki, E., Baba, K., Matsuda, K., Inoue, Y. and Yamakawa, K. (2006) A Kv4.2 truncation mutation in a patient with temporal lobe epilepsy. *Neurobiol. Dis.*, **24**, 245-253.
48. Schrader, L.A., Birnbaum, S.G., Nadin, B.M., Ren, Y., Bui, D., Anderson, A.E. and Sweatt, J.D. (2006) ERK/MAPK regulates the Kv4.2 potassium channel by direct phosphorylation of the pore-forming subunit. *Am. J. Physiol. Cell. Physiol.*, **290**, C852-C861.
49. Petrecca, K., Miller, D.M. and Shrier, A. (2000) Localization and enhanced current density of the Kv4.2 potassium channel by interaction with the actin-binding protein filamin. *J. Neurosci.*, **20**, 8736-8744.

50. Wong, W., Newell, E.W., Jugloff, D.G., Jones, O.T. and Schlichter, L.C. (2002) Cell surface targeting and clustering interactions between heterologously expressed PSD-95 and the *Shal* voltage-gated potassium channel, Kv4.2. *J. Biol. Chem.*, **277**, 20423-20430.
51. Miao, P., Feng, J., Guo, Y., Wang, J., Xu, X., Wang, Y., Li, Y., Gao, L., Zheng, C. and Cheng, H. (2018) Genotype and phenotype analysis using an epilepsy-associated gene panel in Chinese pediatric epilepsy patients. *Clin. Genet.*, **94**, 512-520.
52. Ferri, S.L., Abel, T. and Brodtkin, E.S. (2018) Sex differences in autism spectrum disorder: a review. *Curr. Psychiatry Rep.*, **20**, 9.
53. Shbarou, R. (2016) Current Treatment Options for Early-Onset Pediatric Epileptic Encephalopathies. *Curr. Treat. Options Neurol.*, **18**, 44.
54. Ebbinghaus, J., Legros, C., Nolting, A., Guette, C., Celerier, M.L., Pongs, O. and Bähring, R. (2004) Modulation of Kv4.2 channels by a peptide isolated from the venom of the giant bird-eating tarantula *Theraphosa leblondi*. *Toxicon*, **43**, 923-932.
55. Sanguinetti, M.C., Johnson, J.H., Hammerland, L.G., Kelbaugh, P.R., Volkmann, R.A., Saccomano, N.A. and Mueller, A.L. (1997) Heteropodatoxins: peptides isolated from spider venom that block Kv4.2 potassium channels. *Mol. Pharmacol.*, **51**, 491-498.
56. Maffie, J.K., Dvoretzkova, E., Bougis, P.E., Martin-Eauclaire, M.F. and Rudy, B. (2013) Dipeptidyl-peptidase-like-proteins confer high sensitivity to the scorpion toxin AmmTX3 to Kv4-mediated A-type K⁺ channels. *J. Physiol.*, **591**, 2419-2427.
57. Vacher, H., Diocot, S., Bougis, P.E., Martin-Eauclaire, M.F. and Mourre, C. (2006) Kv4 channels sensitive to BmTX3 in rat nervous system: autoradiographic analysis of their distribution during brain ontogenesis. *Eur. J. Neurosci.*, **24**, 1325-1340.
58. Sobreira, N., Schiettecatte, F., Valle, D. and Hamosh, A. (2015) GeneMatcher: a matching tool for connecting investigators with an interest in the same gene. *Hum. Mutat.*, **36**, 928-930.
59. Long, S.B., Tao, X., Campbell, E.B. and MacKinnon, R. (2007) Atomic structure of a voltage-dependent K⁺ channel in a lipid membrane-like environment. *Nature*, **450**, 376-382.

60. Zhu, X.-R., Wulf, A., Schwarz, M., Isbrandt, D. and Pongs, O. (1999) Characterization of human Kv4.2 mediating a rapidly-inactivating transient voltage-sensitive K⁺ current. *Receptors Channels*, **6**, 387-400.

61. Wada, K., Yokotani, N., Hunter, C., Doi, K., Wenthold, R.J. and Shimasaki, S. (1992) Differential expression of two distinct forms of mRNA encoding members of a dipeptidyl aminopeptidase family. *Proc. Natl. Acad. Sci. U. S. A.*, **89**, 197-201.

62. Firth, H.V., Richards, S.M., Bevan, A.P., Clayton, S., Corpas, M., Rajan, D., Van Vooren, S., Moreau, Y., Pettett, R.M. and Carter, N.P. (2009) DECIPHER: Database of Chromosomal Imbalance and Phenotype in Humans Using Ensembl Resources. *Am J Hum Genet*, **84**, 524-533.

(*) Ref 45: In this review article the V404M variant reported by Lee and co-workers (Ref 34) is erroneously referred to as V404I.

Legends to Figures

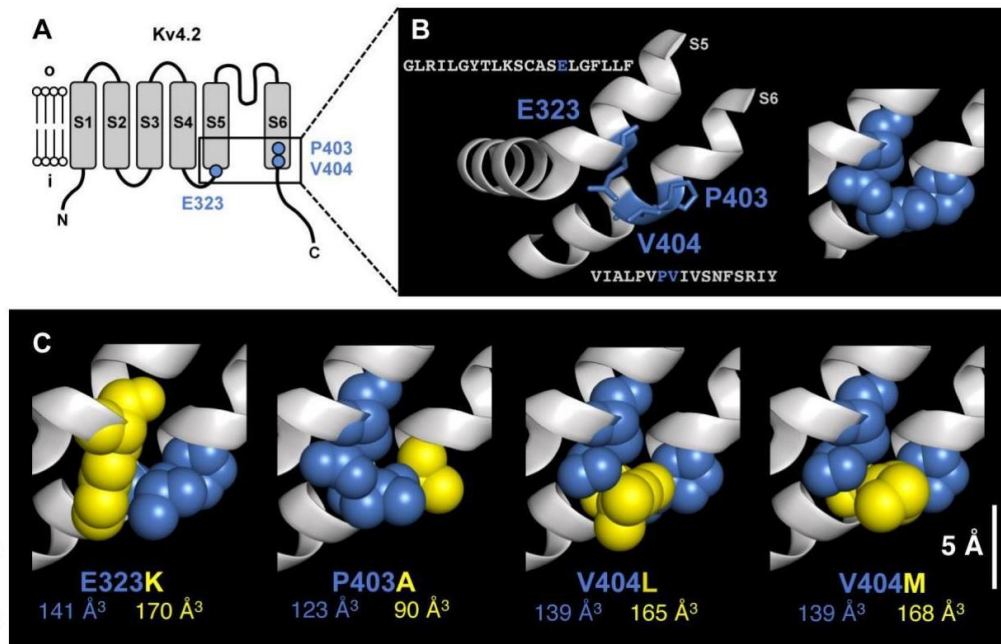


Figure 1: Kv4.2 α -subunit and amino acid substitutions

(A) Scheme of membrane topology of the Kv4.2 α -subunit containing six transmembrane segments (S1 - S6) with a re-entrant loop between S5 and S6 (o: outside; i: inside, with N- and C-terminus). Amino acid residues in the S4S5 linker and the distal S6 segment affected by the reported *KCND2*

variants are indicated (blue circles). **(B)** Topology prediction of S4S5 linker and distal S6 segment. Corresponding Kv4.2 amino acid sequences are shown; protein backbone depicted as ribbon diagram; side chains of E323, P403 and V404 depicted in stick mode (left) and as CPK models (right). **(C)** Mutation-associated amino acid substitutions were simulated with the most likely backbone-dependent rotamer orientation; CPK models of native and novel amino acid side chains shown in blue and yellow, respectively; mean side chain volumes indicated.

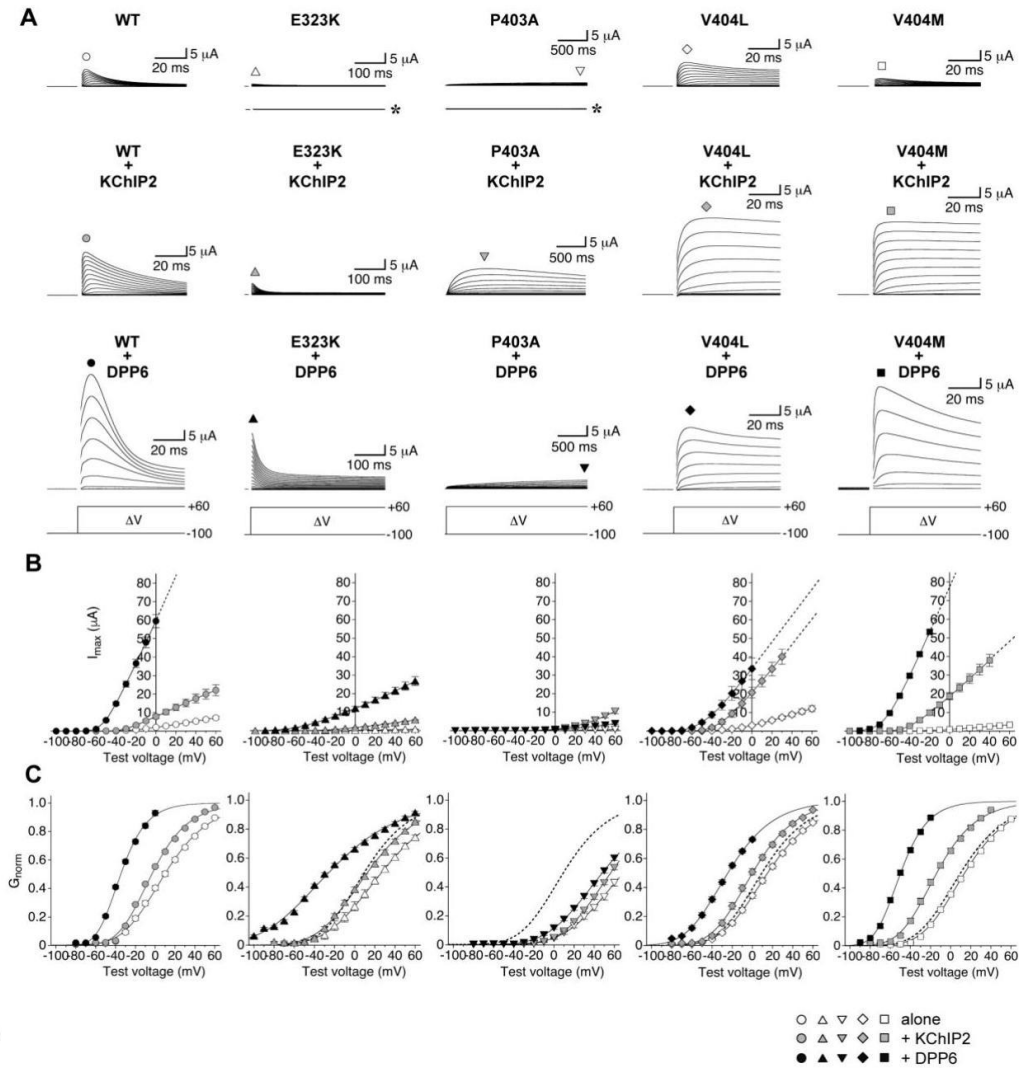


Figure 2: Voltage-dependent activation of Kv4.2 channel variants

Kv4.2 channels were expressed in *Xenopus* oocytes, either alone or in combination with KChIP2 or DPP6, and macroscopic currents were recorded under two-electrode voltage-clamp. **(A)** Current families obtained two days after cRNA injection with pulses from -100 mV to different test voltages between -100 and +60 mV (ΔV : 10 mV increments). Currents are shown for wild-type (WT), E323K,

P403A, V404L and V404M expressed alone, with KChIP2 and with DPP6 (capacitive transients omitted and current traces not shown in full length). Note the different time scales and extremely small current amplitudes for E323K and P403A alone (asterisks: water-injected controls from the same batch of oocytes). **(B)** Current amplitudes (measured at the time points indicated by the symbols in (A)) plotted against test voltage for WT (circles), E323K (triangles), P403A (inverted triangles), V404L (diamonds) and V404M (squares). Data obtained with non-reliable voltage-clamp were omitted; dotted lines: extrapolation drawn by eye. **(C)** Voltage dependence of activation; conductance values were used to generate normalized conductance (G_{norm})-voltage plots for Boltzmann analysis (23, 38). Dotted Boltzmann curves: Kv4.2 WT expressed alone. Empty symbols: channels expressed alone; grey and black symbols: co-expression of KChIP2 and DPP6, respectively.

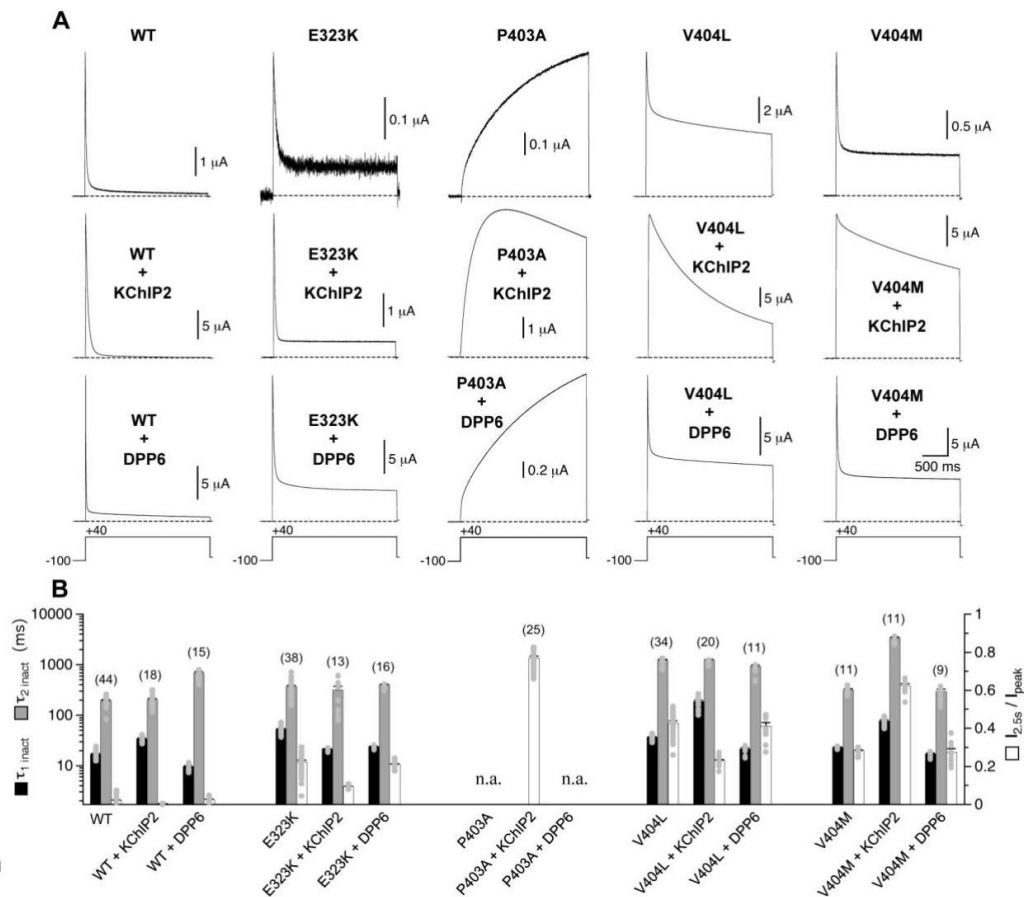


Figure 3: Kinetics of macroscopic inactivation

Modulation of Kv4.2 channel-mediated macroscopic current decay by the mutations and by auxiliary β -subunit co-expression. **(A)** Currents during a 2.5 s test pulse to +40 mV recorded 1 - 3 days after cRNA injection from oocytes expressing Kv4.2 wild-type (WT), E323K, P403A, V404L or V404M in the absence of auxiliary β -subunits, together with KChIP2, or together with DPP6 (dotted line: zero

current). Note that currents mediated by P403A alone and P403A + DPP6 do not reach a maximum during the test pulse. Note also the incomplete current decay for the other mutant channels and the pronounced slowing of current decay for V404L and V404M in the presence of KChIP2. **(B)** Bar graph showing macroscopic inactivation quantified by the time constants obtained with double-exponential fitting (black and grey bars) and the relative current at the end of the test pulse ($I_{2.5s} / I_{peak}$, empty bars); numbers of oocytes (n) indicated; n.a.: not analysed.

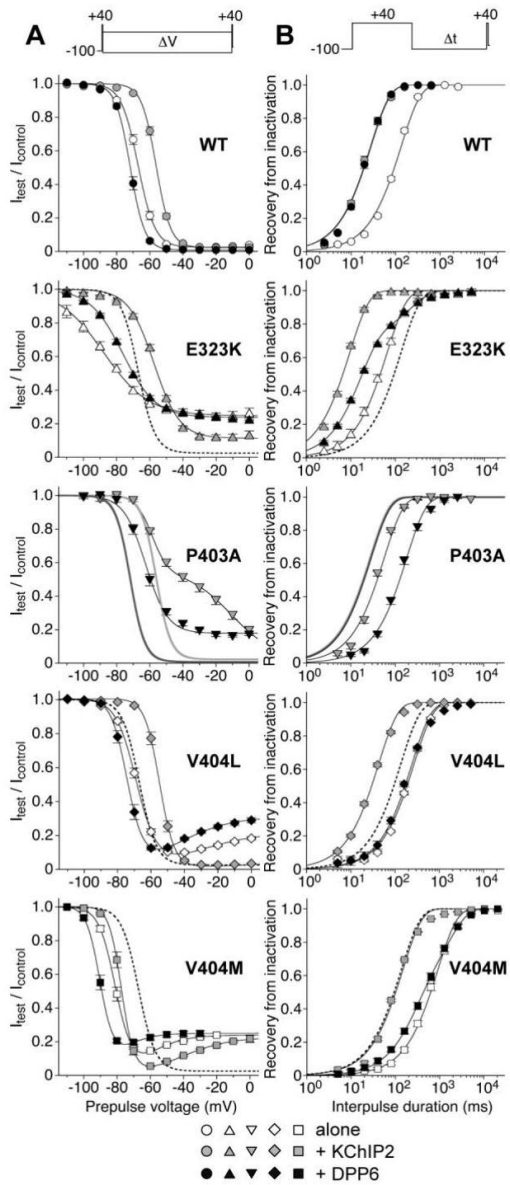


Figure 4: Voltage dependence of steady-state inactivation and recovery kinetics

(A) Voltage dependence of steady-state inactivation for Kv4.2 wild-type (WT) and mutant channels was measured using a double-pulse protocol with a constant interpulse length (10 s) and interpulse

voltages varying between -110 and 0 mV (ΔV : 10 mV increments, see inset). Relative current amplitudes obtained with the second pulse were plotted against prepulse voltage, and data were fitted with a single or, if necessary, the sum of two Boltzmann-functions. Note the biphasic voltage dependencies for P403A + KChIP2, V404L alone and with DPP6, and V404M both in the absence and presence of auxiliary β -subunits. **(B)** Recovery from inactivation was measured using a double-pulse protocol with an interpulse voltage of -100 mV and interpulse durations of ≥ 5 ms (Δt factor = 2, see inset). Relative current amplitudes obtained with the second pulse were plotted against interpulse interval, and the data were fitted with a single- or, if necessary, a double-exponential function. Note the slowed recovery kinetics compared to WT for all mutants except E323K and the moderate effect of DPP6 on the recovery kinetics of V404L and V404M. Empty symbols: channels expressed alone; grey and black symbols: co-expression of KChIP2 and DPP6, respectively; dotted fitting curves: WT expressed alone. Since the voltage dependence of steady-state inactivation and recovery kinetics could not be measured for P403A alone, the fitting curves for WT + KChIP2 and WT + DPP6 (solid light and dark grey lines without symbols, respectively) are shown as reference for P403A + KChIP2 and P403A + DPP6.

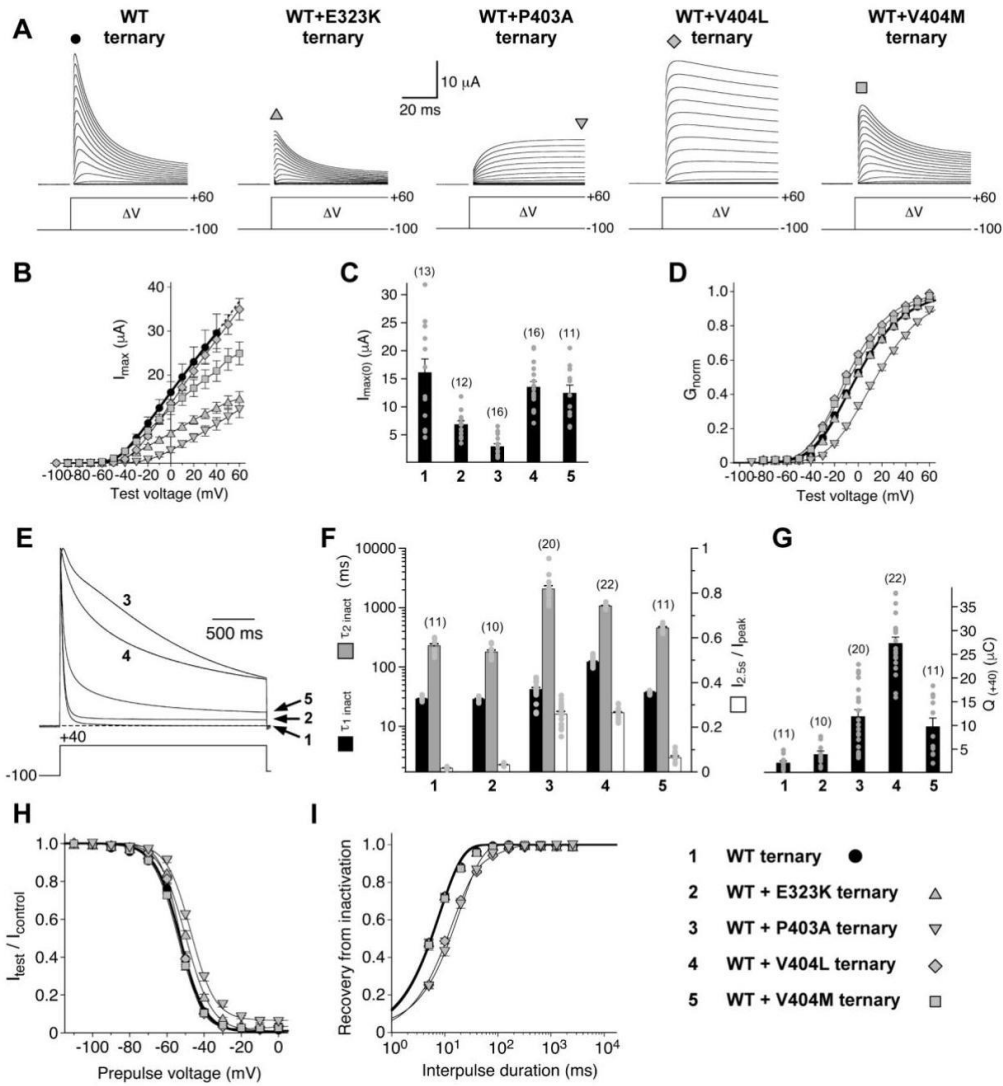


Figure 5: Activation and inactivation of Kv4.2 WT and heteromeric WT + mutant ternary complexes.

Homomeric wild-type (WT) and heteromeric WT + mutant Kv4.2 channels were studied in a ternary configuration with KChIP2 and DPP6. The data are marked by numbers and symbols: (1) WT ternary, circles; (2) WT + E323K ternary, triangles; (3) WT + P403A ternary, inverted triangles; (4) WT + V404L ternary, diamonds; (5) WT + V404M ternary, squares (see also inset on the lower right). **(A)** Current families obtained one day after cRNA injection. **(B)** Current amplitudes (measured at the time points indicated by the symbols in (A) plotted against test voltage. **(C)** Peak current amplitudes measured at a test voltage of 0 mV; numbers of oocytes (n) indicated. **(D)** Normalized conductance (G_{norm})-voltage plots and Boltzmann analysis. **(E)** Currents during a 2.5 s test pulse to +40 mV normalized to peak and overlaid; **(F)** Time constant obtained with double-exponential fitting (black

and grey bars) and the relative current at the end of the test pulse ($I_{2.5s} / I_{peak}$, empty bars); numbers of oocytes (n) indicated; **(G)** Area under the original current traces (i.e., charge at +40 mV during 2.5 s); **(H)** Voltage dependence of steady-state inactivation (data were fitted with a single Boltzmann-function). **(I)** Kinetics of recovery from inactivation (data were fitted with a single or a double-exponential function).

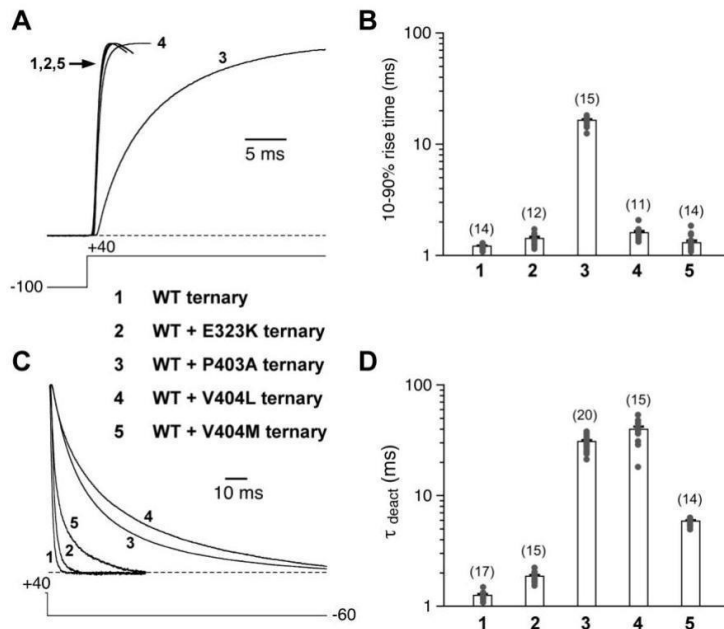


Figure 6: Kinetic analysis of activation and deactivation for Kv4.2 WT and heteromeric WT + mutant ternary complexes

Homomeric wild-type (WT) and heteromeric WT + mutant Kv4.2 channels were studied in a ternary configuration with KChIP2 and DPP6. The data are marked by numbers: (1) WT ternary; (2) WT + E323K ternary; (3) WT + P403A ternary; (4) WT + V404L ternary; (5) WT + V404M ternary. **(A)** Current rising phase at +40 mV; **(B)** 10-90% rise times; **(C)** Tail current relaxation at -60 mV; **(D)** deactivation time constants; numbers of oocytes (n) indicated.

Table 1. Genetic and clinical features of individuals carrying missense mutations in *KCND2*

case	1	2	3	4	5	6
genomic position GRCh38/hg38	chr7:120275 599	chr7:120732 994	chr7:120732 994	chr7:120732 997	chr7:120732 997	chr7:120732 997
mutation in cDNA NM_012281.2	c.967G>A	c.1207C>G	c.1207C>G	c.1210G>T	c.1210G>C	c.1210G>A
amino acid alteration NP_036413	p.Glu323Lys (E323K)	p.Pro403Ala (P403A)	p.Pro403Ala (P403A)	p.Val404Leu (V404L)	p.Val404Leu (V404L)	p.Val404Met

						(V404M)
inheritance	n.d.	n.d.	<i>de novo</i>	<i>de novo</i>	<i>de novo</i>	<i>de novo</i>
zygosity	heterozygous	heterozygous	heterozygous	heterozygous	heterozygous	heterozygous
gnomAD alleles (v2.1.1) *	0	0	0	0	0	0
sex	male	female	female	male	female	female
ethnicity	Caucasian	Caucasian	Native American	Caucasian	Caucasian	Latin American
age at first symptoms	from birth	5 months	< 1 year	6 months	3 months	3 months
current age	13 years	10 years	11 years	2 years 6 months	deceased at the age of 21 years	3 years 6 months
GDD	+	+	+	+	+	+
motor behavior	+	+	+	+	+	+
speech / language	+	+	+	+	+	+
cognition	+	+	+	+	+	+
personal-social	+	n.d.	n.d.	+	+	-
muscle hypotonia	-	+	+	+	+	+
seizures	-	-	-	+	+	+
encephalopathy	n.d.	+	n.d.	+	+	+
autism	-	-	-	+	n.d.	-
visual impairment	-	+	+	-	+	-
brain malformations	n.d.	-	-	-	+	+
physical dysmorphism	-	+	-	-	-	+

+, feature present; -, feature absent; n.d., no data; GDD, global developmental delay

* more than 250,000 alleles analysed

Abbreviations

CSI, closed-state inactivation; DPP, dipeptidyl-peptidase-related protein; ERK, extracellular signal receptor kinase; GDD, global developmental delay; GOF, gain-of-function; KChIP, Kv channel interacting protein; LOF, loss-of-function; PSD-95, post-synaptic density 95; WT, wild-type

1.2 Supplementary material

KCND2 variants associated with
global developmental delay differentially impair Kv4.2 channel gating

Supplementary Material

- Clinical reports
- Supplementary Figures S1, S2, S3 and S4 including legends
- Supplementary Methods
- Supplementary Tables S1 and S2

Clinical reports

Case 1, c.967G>A;p.(Glu323Lys) (E323K), is the third child of non-consanguineous healthy Caucasian parents. He was born at 38 weeks of gestation by elective caesarean section due to a diabetic mother with a birth weight of 5400 grams and a head circumference of 40.5 cm. After birth, he was macrosomic and hypoglycemic and his motor development was delayed. Later, his speech development was delayed and he developed behavioural problems, mainly aggressiveness and getting angry easily. Cognitive tests at the age of 7 years showed a total IQ of 51. He does neither present seizures nor signs of autism spectrum disorder (ASD). Trio whole exome / genome sequencing (WES / WGS) analysis identified a *de novo* missense variant in *KCND2* (NM_012281.3: c.967G>A;p.(Glu323Lys)) while no other likely pathogenic variants were detected.

Case 2, c.1207C>G;p.(Pro403Ala) (P403A), is a Caucasian female born via induced vaginal delivery to a 23 year-old mother at 40 weeks. The pregnancy was complicated by maternal tobacco use, hypertension and proteinuria. The neonatal period was uncomplicated and she passed her newborn hearing screen. The parents noted that she was very fussy and had wandering eye movements soon after birth. She was first evaluated by neurology at six months and found to exhibit global developmental delay (GDD) and hypotonia with poor vision and esophoria. At seven months, a brain MRI was normal and an electroencephalogram (EEG) was consistent with diffuse, mild encephalopathy. At eleven months, an ophthalmological examination revealed decreased visual acuity in both eyes with possible mild optic nerve hypoplasia. In addition, she displayed mild dysmorphisms including a tall forehead, small mouth, high arched palate, a short, small nose, bilateral epicanthal folds and mild two-three toe syndactyly. At 16 months, an abnormal electroretinogram suggested rod/cone dystrophy, while a second brain MRI was normal. At 19 months she was found to have plateauing head circumference, vomiting spells and generalized chorea in addition to the now profound developmental delay, severe visual impairment and significant hypotonia. While her development has thereafter slowly progressed, at the age of 9 years she continues to have very significant global delays, but has not experienced developmental regression. She is able to use a few single-syllable words, knows her name, understands things intermittently, holds her head up and rolls

to move, while her vision progressively declines. Biochemical testing of blood, urine and cerebrospinal fluid revealed no abnormalities. Whole genome sequencing of the child and her father revealed a heterozygous missense variant in *KCND2* (NM_012281.3: c.1207C>G;p.(Pro403Ala)) only present in the child and a paternally inherited frameshift variant in *GUCY2D* (NM_000180.4: c.3018_3024del;p.(Ser1007TrpfsTer12)) with no second hit identified.

Case 3, c.1207C>G;p.(Pro403Ala) (P403A), is a Native American female who presented to genetics clinic in infancy with global developmental delay, hypotonia, microcephaly and cortical visual impairment. Family history was negative for seizures, developmental delay and other neurological conditions. Initial genetic workup included sequencing of *MECP2* and a chromosomal microarray (CMA), both of which were negative. Incidentally CMA revealed regions with loss of heterozygosity (LOH) totaling approximately 8% of the genome. Brain MRI, EEG, and echocardiogram have all been normal. More recently Whole Exome Sequencing revealed a *de novo* VUS (c.1207C>G;p.(Pro403Ala)) in *KCND2* and a variety of other variants in genes that do not fit the patient's phenotype. Patient is now 11 years old and continues to be significantly delayed with severe cognitive impairment. She has persistent hypotonia and is unable to sit or walk on her own. She is wheelchair bound and g-tube dependent. She has approximately 5 words. The patient has visual impairment and continues to have intermittent lateral nystagmus. She had never had a seizure or regression in skills.

Case 4, c.1210G>T;p.(Val404Leu) (V404L), is the first child of non-consanguineous healthy Caucasian parents, born at 40 weeks gestation by normal delivery following a normal pregnancy with a birthweight of 4 kg (P 75), a length of 51 cm (P 50) and an occipitofrontal head circumference (OFC) of 36.5 cm (P 75). His parents reported normal adaptation, feeding and development throughout the first few months of life. At the age of six months, he was admitted to hospital because of mild hypotonia and slightly delayed motor development. No facial dysmorphism was noted. By the age of eight months, he began to have seizures. A brain MRI performed when he was nine months old was normal. However, an EEG showed focal spikes with normal background activity and he was started on levetiracetam. By the age of one year, he experienced a significant increase in seizure

activity including recurrent status epilepticus. Stabilization required triple therapy with valproate, nitrazepam and lamotrigine. EEG analyses continued to show focal epileptic activity only, while his severe hypotonia and generalized developmental delay became increasingly pronounced. Continuous positive airway pressure (CPAP) at night was initiated. Trio whole exome sequencing (WES) for the child and his parents identified a *de novo* missense variant of *KCND2* (NM_012281.2: c.1210G>T;p.Val404Leu), while no other variants of interest were detected, and a 180k array-based comparative genomic hybridization revealed no abnormalities. At the age of two years, he began to develop an epileptic encephalopathy, which did respond to treatment with nitrazepam and valproic acid. His EEG showed both generalized slowing and periodic discharges of generalized spike slow wave complexes, but also periods of slow generalized spike-wave discharges. In addition to poor motor skills and hypotonia, he showed increasing signs of autistic behaviour. At his last review at the age of two and a half years, he had no clinical seizures. However, he could not sit, stand or walk, had not developed any speech and showed poor social skills. His height was 94 cm (P 80), his weight 14.5 kg (P 70) and his OFC 48.5 cm (P 10).

Case 5, c.1210G>C;p.(Val404Leu) (V404L), was a Caucasian female that was born at term after an uneventful pregnancy (birth weight: 3640 g; length: 56 cm; head circumference: 35 cm) as a child of healthy parents and younger sister of two healthy males. First abnormalities were observed at the age of 3 months: lack of fixation, strabismus, muscle hypotonia, no tendency to grab objects, missing head control or any other motor milestone achievement, no spontaneous vocalization (only in pain or discomfort), no visual contact/social interaction. Subsequently, mild hemiparesis was diagnosed. By the age of 8 months and after experiencing repetitive seizures, an EEG examination revealed an early infantile epileptic encephalopathy (hypersynchronous activity patterns with multifocal spikes and sharp-waves with sleep delta waves). Ultrasound and MRI analysis revealed a pronounced cortical frontotemporal brain atrophy with mild expansion of inner liquor spaces. Little myelination was diagnosed along the visual tract. The patient died at the age of 21 years of an unknown cause. Post-mortem trio WES revealed three heterozygous *de novo* variants, all of which were neither found in both parents nor the healthy older brother (*KCND2*, NM_012281.3: c.1210G>C;p.(Val404Leu),

OR4K14, NM_001004712.2: c.197A>G;p.(Asn66Ser), *PRDM2*, NM_012231.4: c.3155C>T;p.(Ser1052Phe)).

Case 6, c.1210G>A;p.(Val404Met) (V404M), underwent panel testing of 187 genes associated with epilepsy and was found to harbor a *KCND2* variant. Subsequent parental testing, including confirmation of maternity and paternity using informative SNPs, confirmed the variant was *de novo*. She began having seizures at the age of three months at which time she was started on levetiracetam. Valproic acid was added after two months and she remained on this combination for approximately one year. Seizures then recurred and topiramate was added. She displays three types of seizures: 1) behavioral arrest, with left eye straight ahead and right eye deviating to right, with tremulousness or brief right arm jerks lasting for 10-15 seconds; 2) generalized facial twitching persisting for some seconds; 3) generalized convulsions continuing for up to 15 seconds. Routine EEG showed some generalized spikes with focal onset (occipital regions independently). Brain MRI at five months of age showed lower white matter volume in periventricular regions of occipital lobes but no evidence of hippocampal atrophy. A second MRI did not reveal any cortical malformations, but showed prominent ventricles and a decrease in deep white matter. In addition, she presents with global developmental delay and hypotonia, but continues to make slow developmental gains. She is able to take a few independent steps, climb onto furniture and crawl. She babbles spontaneously, smiles, gestures inconsistently and waves “bye” inconsistently. She receives physical, occupational, speech and developmental therapies weekly. She was diagnosed with hypothyroidism and started on levothyroxine. She also has mild dysmorphic features described as deep set almond shaped eyes, a pointed chin, a prominent brow ridge, a small nose, large anteriorly rotated ears and a tall forehead.

Abbreviations used: ASD, autism spectrum disorder; CMA, chromosomal microarray; CPAP, continuous positive airway pressure; EEG, electroencephalogram; GDD, global developmental delay; LOH, loss of heterozygosity; MRI, magnetic resonance imaging; OFC, occipitofrontal head circumference; SNP, single-nucleotide polymorphism; VUS, variant of uncertain significance; WES / WGS, whole exome / genome sequencing

Gene	Protein		S4S5 linker		S6
<i>KCNA1</i>	Kv 1.1	311	GLQILGQTLKASMR EL GLLLIF	331	399 TIAL PV PVIVSNFNIFY 415
<i>KCNB1</i>	Kv 2.1	316	GLQSLGFTLRRSY NE LGLLIL	336	404 VIAL PI PIIVNNFSEFY 420
<i>KCNC1</i>	Kv 3.1	330	GLRVLGHTLRAS TNE FLLLI	350	427 TIAMP PV PVIVNNFGMY 443
<i>KCND1</i>	Kv 4.1	311	GLRILGYTLKSCAS EL GFLLF	313	399 VIAL PV PVIVSNFSRIY 415
<i>KCND2</i>	Kv 4.2	309	GLRILGYTLKSCASELGFLLF	329	397 VIALPVPVIVSNFSRIY
<i>KCND3</i>	Kv 4.3	306	GLRILGYTLKSCAS EL GFLLF	326	394 VIAL PV PVIVSNFSRIY 410
<i>KCNF1</i>	Kv 5.1	309	GLQTLTYALKRS FK ELGLLM	329	397 AIAL PI PIIINNFRVRY 413
<i>KCNG1</i>	Kv 6.1	362	GLQTLGLTARRC TR EFGLLL	382	451 LMAFP V TSIFHTFSRSY 467
<i>KCNQ1</i>	Kv 7.1	247	TWRLLGSVVF IHRQ ELITTL	267	339 FFAL PA GIILGSGFALKV 355
<i>KCNV1</i>	Kv 8.1	331	GLRSLGMT IT QCY EV GLLLL	351	419 VLAL PI AIINDRFSACY 435
<i>KCNS1</i>	Kv 9.1	361	GLRSLGATLKHSY RE VGILL	381	448 VVAL PI TIIFNKFSHFY 464
<i>KCNH1</i>	Kv10.1	369	-----DHY I EYGA AVL	379	490 LYAT IF GNVTIFQOMY 506
<i>KCNH2</i>	Kv11.1	540	-----DRY S EYGA AVL	550	651 MYAS IF GNVSIIQRLY 667
<i>KCNH8</i>	Kv12.1	346	-----DRY S QHSTIVL	356	461 MHAL V FGNVTAIQRM 477

Figure S1: Sequence alignment of Kv superfamily members

Single letter code alignment of human Kv superfamily members Kv1 - Kv12 covering the S4S5 linker and the distal S6 segment (residue numbers for the first and last amino acid within the shown segments are indicated; generated with UniProt; <https://www.uniprot.org/>). The first representative of each subfamily and all members of the Kv4 subfamily (Kv4.2 in bold) are shown, including the respective approved gene symbols. The displayed regions are highly conserved and 100% identical within the Kv4 subfamily. However, subfamily members Kv10 - Kv12 lack an equivalent to the N-terminal half of the S4S5 linker. The glutamate residue in the S4S5 linker (E323 in Kv4.2, blue; affected in case 1 of the present study) is conserved throughout the Kv superfamily, except for Kv12.1. The conserved PXP motif, critically involved in operating the cytoplasmic S6 gate in subfamilies Kv1 - Kv4, is indicated. The second proline - valine (PV) repeat (P403 and V404 in Kv4.2, blue; affected in case 2 and 3 and in case 4 - 6, respectively, of the present study) is conserved within subfamilies Kv1 - Kv4, except for Kv2.1. Non-conserved residues are shown in magenta.

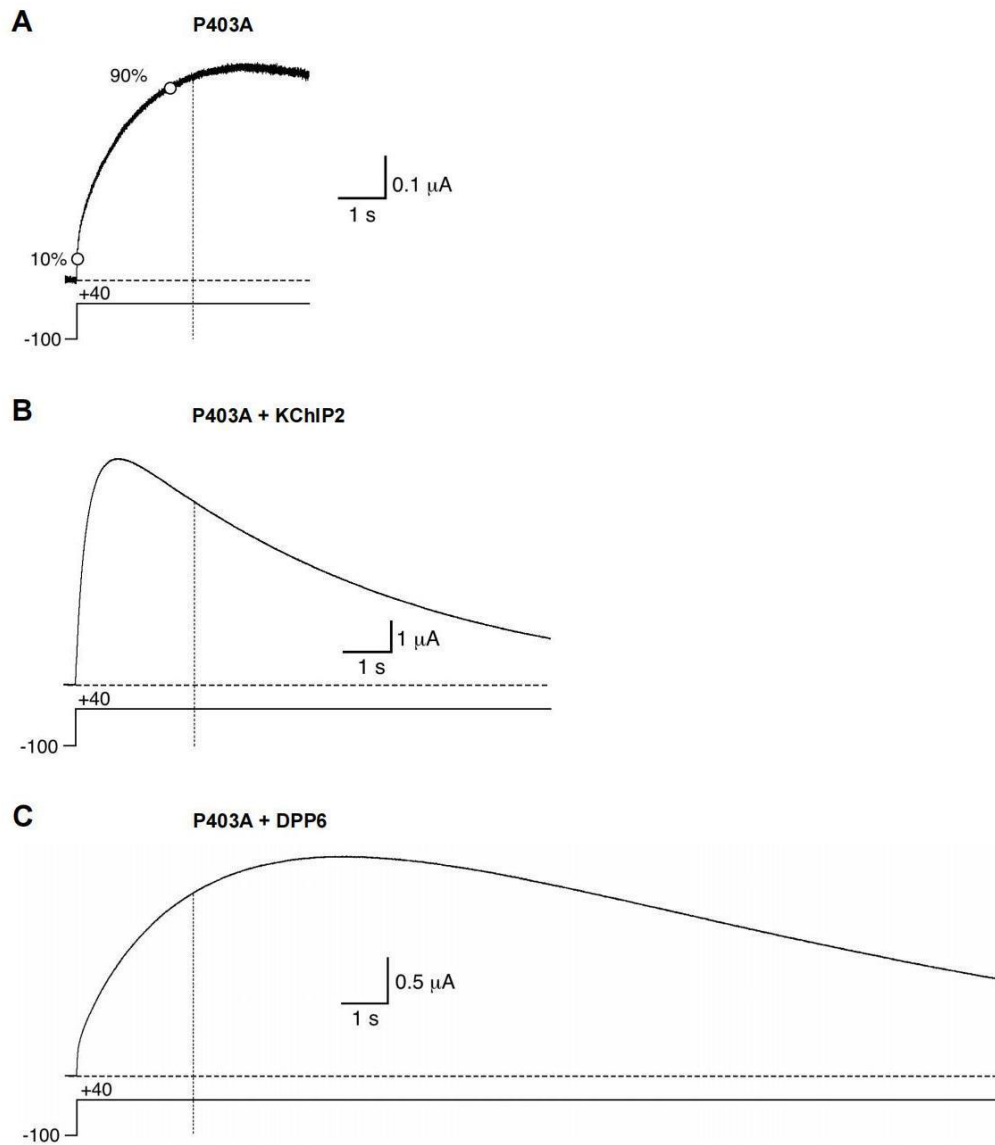
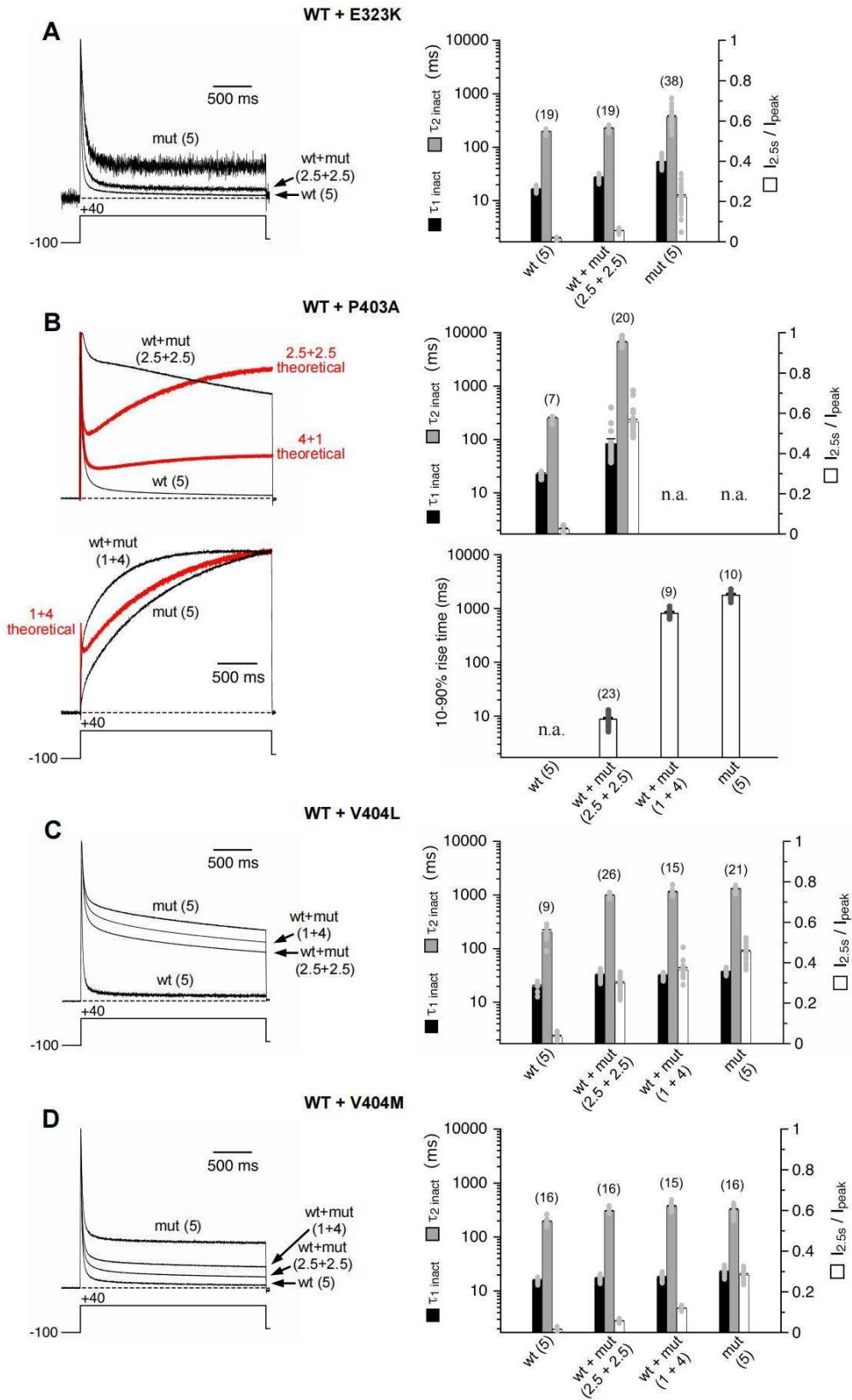


Figure S2: Kv4.2 P403A currents elicited by extended voltage pulses

Currents mediated by P403A alone (**A**), P403A co-expressed with KChIP2 (**B**) and P403A co-expressed with DPP6 (**C**) were activated by voltage pulses longer than 2.5 s (vertical dotted lines) to +40 mV; horizontal dotted lines: zero current. The results obtained with voltage pulses lasting 10 - 20 s suggest that macroscopic inactivation exists for P403A + KChIP2 and for Kv4.2 P403A + DPP6. Extended voltage pulses also revealed an apparent current decay for P403A alone but the small amplitude of these currents precluded a systematic study of inactivation, as stated earlier (Barghaan & Bähring, *J Gen Physiol* 133, 205-224, 2009). The 10-90% rise time analysis is illustrated in A.



Zhang et al., Figure S3

Figure S3: Currents mediated by heteromeric WT + mutant Kv4.2 channels

Heteromeric Kv4.2 channel formation was induced by co-injecting wild-type (wt) and mutant (mut) cRNAs (encoding E323K, P403A, V404L or V404M) at equal cRNA amounts or at a 4-fold excess of mut. Currents recorded during a 2.5 s testpulse to +40 mV were normalized to peak and overlaid. It was tested whether and how the currents mediated by the heteromers differed from the ones recorded from oocytes injected with wt or mut alone; current traces are labeled accordingly, and respective cRNA amounts (in ng per oocyte) are indicated. For WT + P403A the theoretical sum of averaged WT and mut currents at the indicated ratios was calculated (red traces). Macroscopic inactivation is approximated by a double-exponential function (time constants depicted by black and grey bars) and by the relative current at the end of the test pulse ($I_{2.5s} / I_{peak}$, empty bars). For homomeric and heteromeric P403A the current activation kinetics are quantified by the 10-90% rise time (empty bars); number of oocytes (n) indicated; n.a.: not analysed.

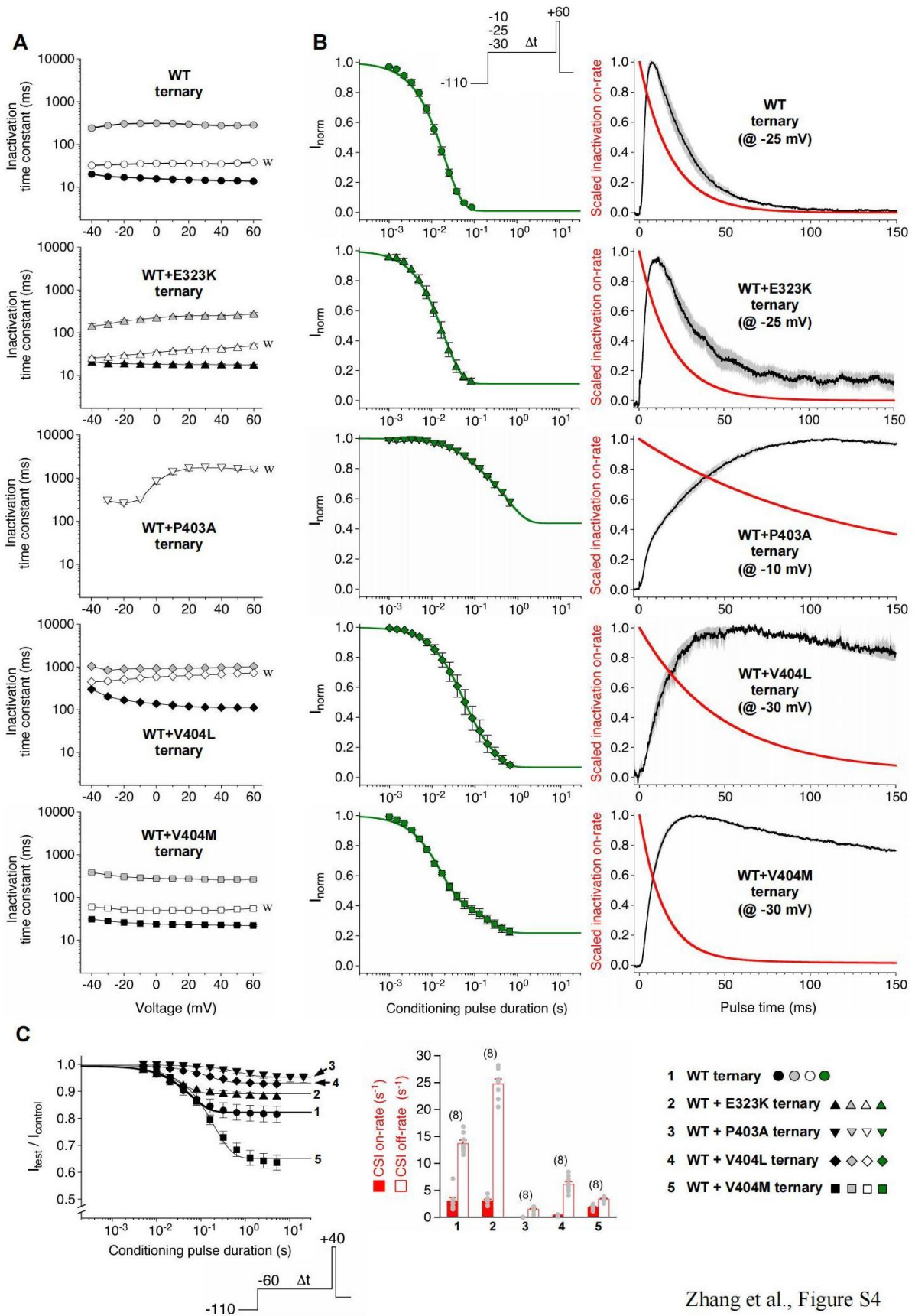


Figure S4: Closed-state inactivation in ternary Kv4.2 channels

Homomeric WT ternary and heteromeric WT + mutant ternary channels were tested for preferential closed-state inactivation (CSI). **(A)** Voltage dependence of macroscopic inactivation kinetics; time constants obtained with double-exponential fitting (black and grey symbols) and weighted time constants (empty symbols) are plotted against test voltage. **(B)** The onset of inactivation at moderate depolarization was measured with a conditioning pulse protocol in the cell-attached configuration of the patch-clamp technique (see inset and Supplementary Methods). The relative test pulse current amplitudes were plotted against the conditioning pulse duration, and the onset kinetics of inactivation were analysed with appropriate exponential functions (green curves). The negative first derivatives of these curves were calculated, scaled and plotted superimposed on the current trace obtained with the same conditioning pulse at maximal length (red). **(C)** Onset of CSI was measured with a conditioning pulse protocol (-60 mV, see inset). The relative test pulse current amplitudes were plotted against the conditioning pulse duration and the onset kinetics of CSI were analysed with a single-exponential function. From the obtained data CSI on-rates and CSI off-rates were calculated (see Supplementary Methods).

Supplementary Methods

Additional voltage-clamp recordings and data analysis

Patch-clamp recordings were performed in the cell-attached configuration (Chabala et al, J Gen Physiol 102, 713-728, 1993; Fineberg et al, J Gen Physiol 140, 513-527, 2012) on devitellinized oocytes expressing homomeric WT ternary or heteromeric WT + mutant ternary channels (Supplementary Material, Fig. S4B). The oocytes were bathed in a solution containing (in mM) 140 K-aspartate, 10 KCl, 1.8 CaCl₂ and 10 HEPES (pH 7.2, KOH; oocyte resting potential near 0 mV). Patch pipettes were pulled from thick-walled glass, fire-polished, and filled with a solution containing (in mM) 96 NaCl, 2 KCl, 1.8 CaCl₂, 1 MgCl₂ and 5 HEPES (pH 7.4, NaOH; tip resistances between 600 and 800 kΩ). Macropatches were voltage-clamped with an EPC9 patch-clamp amplifier (HEKA). Signals were filtered with low-pass Bessel characteristics, sampled at 10 kHz, and a p/5 protocol was used for leak subtraction. We applied conditioning pulses of different length followed by a test pulse to +60 mV. The conditioning pulses (-30, -25 or -10 mV) activated roughly 20% of the maximal conductance (as deduced from the data in Fig. 5D). The onset kinetics of inactivation during the conditioning pulse were fitted with appropriate exponential functions. The negative first derivative of this function represents the rate of inactivation (Bean, Biophys J 35, 595-614, 1981; Fineberg et al, J Gen Physiol 140, 513-527, 2012). In the presence of considerable CSI the rate of inactivation (red curve) does not correlate (i.e., superimpose) with the current trace, directly reflecting open probability. Oocytes expressing ternary channels were also tested under two-electrode voltage-clamp (see Materials and Methods), by applying conditioning pulses of different length to -60 mV followed by a test pulse to +40 mV. Here, the conditioning pulse induced negligible open probability (Fig. 5D). The onset kinetics of closed-state inactivation (CSI) were described by a single-exponential function. Based on the obtained time constant (τ_{-60}) and the fraction non-inactivated (f) CSI on-rates and CSI off-rates were calculated according to the following equations: CSI off-rate = f / τ_{-60} ; CSI on-rate = $1 / \tau_{-60} - \text{CSI off-rate}$ (Barghaan & Bähring, J Gen Physiol 133, 205-224, 2009).

Table S1. Activation and deactivation parameters for wild-type and mutant Kv4.2 channels in the absence and presence of auxiliary subunits.

Kv4.2	$I_{\max(0)}$ on day 2 (μA)	$Q_{(+40)}$ on day 1 (μC)	$V_{1/2 \text{ act}}$ (mV)	k_{act} (mV)	10-90% rise time (ms)	τ_{deact} (ms)
WT	2.06 ± 0.26 (n=14)		$+9.60 \pm 1.55$ (n=16)	28.2 ± 0.3 (n=16)		
E323K	$0.28 \pm 0.02^{\text{mm}}$ (n=17)		$+21.3 \pm 2.9^{\text{m}}$ (n=11)	$36.1 \pm 2.1^{\text{mm}}$ (n=11)		
P403A	$0.12 \pm 0.004^{\text{mm}}$ (n=14)		$+69.3 \pm 3.0^{\text{mm}}$ (n=3)	$38.7 \pm 1.8^{\text{m}}$ (n=3)	1760 ± 110 (n=10)	
V404L	$3.04 \pm 0.38^{\text{m}}$ (n=12)		$+15.3 \pm 1.7$ (n=12)	30.3 ± 0.4 (n=12)		
V404M	$0.90 \pm 0.11^{\text{m}}$ (n=8)		$+13.3 \pm 1.2$ (n=8)	28.3 ± 0.5 (n=8)		
WT+KChIP2	$7.90 \pm 1.11^{\text{k}}$ (n=9)		$-3.52 \pm 0.76^{\text{kk}}$ (n=15)	$23.1 \pm 0.5^{\text{kk}}$ (n=15)		
E323K+KChIP2	$1.69 \pm 0.08^{\text{kk}}$ (n=15)		$+12.7 \pm 1.6^{\text{k}}$ (n=18)	32.8 ± 0.6 (n=18)		
P403A+KChIP2	$0.77 \pm 0.10^{\text{kk}}$ (n=19)		$+56.9 \pm 1.4^{\text{k}}$ (n=19)	32.5 ± 0.7 (n=19)		
V404L+KChIP2	$20.8 \pm 2.8^{\text{kk}}$ (n=5)		$+0.41 \pm 1.91^{\text{kk}}$ (n=13)	$26.4 \pm 0.4^{\text{kk}}$ (n=13)		
V404M+KChIP2	$18.7 \pm 1.9^{\text{kk}}$ (n=8)		$-13.9 \pm 1.9^{\text{kk}}$ (n=8)	$24.5 \pm 0.2^{\text{kk}}$ (n=8)		
WT+DPP6	$59.6 \pm 3.6^{\text{dd}}$ (n=21)		$-31.2 \pm 1.1^{\text{dd}}$ (n=20)	$20.3 \pm 1.0^{\text{dd}}$ (n=20)		
E323K+DPP6	$12.0 \pm 1.1^{\text{dd}}$ (n=15)		$-25.5 \pm 1.5^{\text{dd}}$ (n=15)	$44.4 \pm 1.5^{\text{d}}$ (n=15)		
P403A+DPP6	$0.58 \pm 0.09^{\text{d}}$ (n=14)		$+48.3 \pm 1.8^{\text{d}}$ (n=14)	36.0 ± 0.7 (n=14)		
V404L+DPP6	$29.4 \pm 4.6^{\text{d}}$ (n=9)		$-24.4 \pm 1.5^{\text{dd}}$ (n=20)	$28.1 \pm 0.9^{\text{d}}$ (n=20)		
V404M+DPP6	-78.5 (n=8)		$-49.9 \pm 1.2^{\text{dd}}$ (n=8)	$18.7 \pm 1.2^{\text{dd}}$ (n=8)		
WT+P403A (2.5+2.5)					$8.73 \pm 0.52^{\text{hh}}$ (n=23)	
WT+P403A (1+4)					$810 \pm 53^{\text{hh}}$ (n=9)	
WT ternary	16.1 ± 2.4 (n=13)	2.10 ± 0.40 (n=11)	-0.89 ± 1.61 (n=10)	24.8 ± 0.6 (n=10)	1.21 ± 0.02 (n=14)	1.26 ± 0.03 (n=17)
WT+E323K ternary	$6.85 \pm 0.67^{\text{t}}$ (n=12)	3.90 ± 0.70 10	-0.81 ± 1.16 (n=10)	23.8 ± 0.3 (n=10)	1.42 ± 0.05 (n=12)	1.87 ± 0.05 (n=15)
WT+P403A ternary	$2.90 \pm 0.49^{\text{tt}}$ (n=16)	$11.9 \pm 1.5^{\text{tt}}$ (n=20)	$+14.7 \pm 1.4^{\text{tt}}$ (n=16)	25.9 ± 0.4 (n=16)	$16.4 \pm 0.4^{\text{t}}$ (n=15)	$30.7 \pm 1.0^{\text{n}}$ (n=20)
WT+V404L ternary	13.5 ± 1.0 (n=16)	$27.3 \pm 1.3^{\text{tt}}$ (n=22)	$-9.75 \pm 0.71^{\text{tt}}$ (n=18)	$22.4 \pm 0.4^{\text{t}}$ (n=18)	1.60 ± 0.06 (n=11)	$39.8 \pm 2.3^{\text{tt}}$ (n=15)
WT+V404M ternary	12.4 ± 1.4 (n=11)	$9.75 \pm 1.80^{\text{t}}$ (n=11)	$-6.96 \pm 0.90^{\text{t}}$ (n=11)	24.0 ± 0.3 (n=11)	1.30 ± 0.06 (n=14)	$5.87 \pm 0.12^{\text{t}}$ (n=14)

Analysis results obtained for the maximal current amplitude at 0 mV ($I_{\max(0)}$) measured on day 2, the integral under the current trace ($Q_{(+40)}$) on day 1, the voltage of half-maximal activation ($V_{1/2 \text{ act}}$) including the corresponding slope factor (k_{act}), the 10-90% rise time and the deactivation time constant (τ_{deact}); data given as mean \pm SEM; number of oocytes (n) indicated.

Statistical analyses were done using one-way analysis of variance (ANOVA) with Dunnett's post hoc testing for more than two groups and Student's t-test for two groups. Letters m, k, d, h and t denote significant differences; single letter: $p < 0.05$; two letters: $p < 0.0001$; m, mm: significantly different from Kv4.2 WT alone (mutant effect); k, kk: significantly different in the presence of KChIP2; d, dd: significantly different in the presence of DPP6; h, hh: significantly different from Kv4.2 P403A alone if Kv4.2 WT is co-expressed; t, tt: significantly different from Kv4.2 WT ternary.

Based on the statistical analysis results, significant mutant-related features in the ternary complexes compatible with loss-of-function (LOF, red) and gain-of-function (GOF, green) are indicated.

Table S2. Inactivation parameters for wild-type and mutant Kv4.2 channels in the absence and presence of auxiliary subunits.

Kv4.2	$\tau_{1 \text{ inact}}$ (ms)	amp ₁ (%)	$\tau_{2 \text{ inact}}$ (ms)	amp ₂ (%)	I _{2.5s} / I _{peak}	V _{1/2 inact} (mV)	k _{inact} (mV)	τ_{rec} (ms)
WT	16.9 ± 0.4 (n=44)	92.6 ± 0.2 (n=44)	197 ± 5 (n=44)	7.4 ± 0.2 (n=44)	0.022 ± 0.002 (n=44)	-68.0 ± 0.5 (n=30)	5.20 ± 0.15 (n=30)	146 ± 5 (n=26)
E323K	52.9 ± 1.5 ^{mm} (n=38)	87.0 ± 1.7 ^m (n=38)	369 ± 21 ^{mm} (n=38)	13.0 ± 1.7 ^m (n=38)	0.223 ± 0.010 ^{mm} (n=38)	-86.5 ± 1.5 ^{mm} (n=9)	11.3 ± 1.0 ^{mm} (n=9)	76.0 ± 6.9 (n=15)
P403A								
V404L	37.0 ± 0.7 ^{mm} (n=34)	71.8 ± 0.8 ^{mm} (n=34)	1239 ± 26 ^{mm} (n=34)	28.2 ± 0.8 ^{mm} (n=34)	0.431 ± 0.010 ^{mm} (n=34)	-68.9 ± 0.7 (n=21)	5.78 ± 0.15 (n=21)	281 ± 18 ^{aa} (n=19)
V404M	23.0 ± 0.3 ^m (n=11)	92.6 ± 0.1 (n=11)	318 ± 16 ^m (n=11)	7.4 ± 0.1 (n=11)	0.283 ± 0.005 ^{mm} (n=11)	-81.2 ± 0.9 ^{mm} (n=9)	5.10 ± 0.09 (n=9)	939 ± 88 ^{mm} (n=9)
WT+KChIP2	34.3 ± 1.1 ^{kk} (n=18)	89.2 ± 1.1 ^k (n=18)	202 ± 15 (n=18)	10.8 ± 1.1 ^k (n=18)	0.004 ± 0.001 ^{kk} (n=18)	-56.2 ± 0.5 ^{kk} (n=15)	4.28 ± 0.11 ^{kk} (n=15)	27.8 ± 1.9 ^{kk} (n=17)
E323K+KChIP2	21.5 ± 0.4 ^{kk} (n=13)	98.8 ± 0.2 ^{kk} (n=13)	317 ± 61 (n=13)	1.2 ± 0.2 ^{kk} (n=13)	0.094 ± 0.003 ^{kk} (n=13)	-57.4 ± 0.7 ^{kk} (n=12)	7.71 ± 0.18 ^k (n=12)	10.3 ± 0.3 ^{kk} (n=13)
P403A+KChIP2					0.769 ± 0.010 ^{aa} (n=27)	-58.9 ± 0.5 ^a (n=14)	5.56 ± 0.61 (n=14)	56.6 ± 2.1 ^{aa} (n=10)
V404L+KChIP2	188 ± 10 ^{kk} (n=20)	8.7 ± 0.6 ^{kk} (n=20)	1261 ± 20 (n=20)	91.3 ± 0.6 ^{kk} (n=20)	0.231 ± 0.005 ^{kk} (n=20)	-55.1 ± 0.8 ^{kk} (n=11)	3.91 ± 0.17 ^{kk} (n=11)	42.6 ± 2.4 ^{kk} (n=14)
V404M+KChIP2	77.2 ± 4.3 ^{kk} (n=11)	11.6 ± 1.4 ^{kk} (n=11)	3440 ± 116 ^{kk} (n=11)	88.4 ± 1.4 ^{kk} (n=11)	0.624 ± 0.010 ^{kk} (n=11)	-67.5 ± 0.8 ^{kk} (n=8)	3.52 ± 0.03 ^{kk} (n=8)	146 ± 4 ^{kk} (n=8)
WT+DPP6	9.63 ± 0.39 ^{dd} (n=15)	96.8 ± 0.2 ^{dd} (n=15)	699 ± 28 ^{dd} (n=15)	3.2 ± 0.2 ^{dd} (n=15)	0.026 ± 0.003 (n=15)	-71.8 ± 0.7 ^d (n=13)	4.12 ± 0.06 ^{dd} (n=13)	27.7 ± 1.8 ^{dd} (n=14)
E323K+DPP6	23.8 ± 0.4 ^{dd} (n=16)	91.8 ± 0.2 ^d (n=16)	399 ± 9 (n=16)	8.2 ± 0.2 ^d (n=16)	0.210 ± 0.005 (n=16)	-75.7 ± 0.6 ^{dd} (n=10)	10.3 ± 0.1 (n=10)	19.8 ± 0.55 ^{dd} (n=9)
P403A+DPP6						-62.0 ± 1.1 ^{aa} (n=10)	7.78 ± 0.30 ^{aa} (n=10)	186 ± 12 ^{aa} (n=10)
V404L+DPP6	21.4 ± 1.1 ^{dd} (n=11)	85.2 ± 1.6 ^{dd} (n=11)	924 ± 62 ^d (n=11)	14.8 ± 1.6 ^{dd} (n=11)	0.411 ± 0.021 (n=11)	-74.5 ± 1.0 ^{dd} (n=13)	4.42 ± 0.15 ^{dd} (n=13)	254 ± 14 (n=15)
V404M+DPP6	17.0 ± 0.6 ^{dd} (n=9)	93.9 ± 0.3 ^d (n=9)	295 ± 32 (n=9)	6.1 ± 0.3 ^d (n=9)	0.275 ± 0.020 (n=9)	-90.3 ± 0.9 ^{dd} (n=9)	3.93 ± 0.12 ^{dd} (n=9)	309 ± 36 ^{dd} (n=8)
WT+E323K (2.5+2.5)	27.2 ± 0.7 (n=19)	87.7 ± 0.2 ^{hh} (n=19)	226 ± 5 (n=19)	12.3 ± 0.2 ^{hh} (n=19)	0.054 ± 0.002 ^h (n=19)			
WT+P403A (2.5+2.5)	84.6 ± 19.4 ^{hh} (n=20)	28.7 ± 1.3 ^{hh} (n=20)	6701 ± 223 ^{hh} (n=20)	71.3 ± 1.3 ^{hh} (n=20)	0.556 ± 0.014 ^{hh} (n=20)			
WT+V404L (2.5+2.5)	32.3 ± 0.8 (n=26)	79.0 ± 0.7 ^{hh} (n=26)	988 ± 12 ^{hh} (n=26)	21.0 ± 0.7 ^{hh} (n=26)	0.298 ± 0.007 ^{hh} (n=26)			
WT+V404L (1+4)	31.8 ± 0.9 (n=15)	77.2 ± 1.2 ^{hh} (n=15)	1133 ± 35 ^{hh} (n=15)	22.8 ± 1.2 ^{hh} (n=15)	0.365 ± 0.011 ^{hh} (n=15)			
WT+V404M (2.5+2.5)	17.4 ± 0.5 (n=16)	92.1 ± 0.4 (n=16)	303 ± 8 (n=16)	7.9 ± 0.4 (n=16)	0.058 ± 0.002 ^h (n=16)			
WT+V404M (1+4)	18.1 ± 0.6 (n=15)	92.1 ± 0.4 (n=15)	372 ± 13 (n=15)	7.9 ± 0.4 (n=15)	0.120 ± 0.002 ^{hh} (n=15)			
WT ternary	28.8 ± 0.8 (n=11)	94.1 ± 0.4 (n=11)	227 ± 19 (n=11)	5.9 ± 0.4 (n=11)	0.016 ± 0.002 (n=11)	-53.1 ± 0.8 (n=10)	6.32 ± 0.11 (n=10)	7.99 ± 0.44 (n=10)
WT+E323K ternary	28.7 ± 0.8 (n=10)	93.1 ± 0.4 (n=10)	179 ± 14 (n=10)	6.9 ± 0.4 (n=10)	0.031 ± 0.002 (n=10)	-49.9 ± 0.5 (n=10)	6.32 ± 0.11 (n=10)	7.89 ± 0.39 (n=10)
WT+P403A ternary	41.8 ± 3.1 ^t (n=20)	26.9 ± 3.4 ^{tt} (n=20)	2065 ± 283 ^{tt} (n=20)	73.1 ± 3.4 ^{tt} (n=20)	0.259 ± 0.012 ^{tt} (n=20)	-46.9 ± 0.7 ^{tt} (n=25)	6.97 ± 0.19 (n=25)	17.6 ± 1.4 ^{tt} (n=25)
WT+V404L ternary	121 ± 4 ^{tt} (n=22)	35.0 ± 0.3 ^{tt} (n=22)	1066 ± 18 ^t (n=22)	65.0 ± 0.3 ^{tt} (n=22)	0.264 ± 0.005 ^{tt} (n=22)	-52.4 ± 0.8 (n=18)	5.03 ± 0.17 ^{tt} (n=18)	18.3 ± 0.7 ^{tt} (n=18)
WT+V404M ternary	37.5 ± 0.7 (n=11)	76.3 ± 1.1 ^{tt} (n=11)	456 ± 22 (n=11)	23.7 ± 1.1 ^{tt} (n=11)	0.064 ± 0.008 ^t (n=11)	-54.3 ± 0.6 (n=10)	6.26 ± 0.14 (n=10)	8.29 ± 0.55 (n=11)

Analysis results obtained for the time constants of macroscopic inactivation ($\tau_{1 \text{ inact}}$ and $\tau_{2 \text{ inact}}$) and their relative amplitudes (amp₁ and amp₂, respectively), the relative current at the end of a 2.5 s test pulse (I_{2.5s} / I_{peak}), the voltage of half-maximal inactivation (V_{1/2 inact}) including the corresponding slope factor (k_{inact}) and the time constant of recovery from inactivation (τ_{rec}); data given as mean ± SEM; number of oocytes (n) indicated.

Statistical analyses were done using one-way analysis of variance (ANOVA) with Dunnett's post hoc testing for more than two groups and Student's t-test for two groups. Letters m, a, k, d, h and t denote significant differences; single letter: p < 0.05; two letters: p < 0.0001; m, mm: significantly different from Kv4.2 wt alone (mutant effect); a, aa: significantly different from Kv4.2 WT + KChIP2 or Kv4.2 WT + DPP6 (P403A effects analysed in the presence of KChIP2 or DPP6); k, kk: significantly different in the presence of KChIP2; d, dd: significantly different in the presence of DPP6; h, hh: significantly different from Kv4.2 WT if mutant is co-expressed; t, tt: significantly different from Kv4.2 WT ternary.

Based on the statistical analysis results significant mutant-related features in the ternary complexes compatible with loss-of-function (LOF, red) and gain-of-function (GOF, green) are indicated.

1.3 Letter of acceptance

Von Human Molecular Genetics <onbehalf@manuscriptcentral.com> ☆

Betreff Human Molecular Genetics HMG-2021-D-00132.R2

08.07.21, 00:05

Antwort an hmg.editorialoffice@oup.com ☆

An Mich ★

07-Jul-2021

Manuscript number: HMG-2021-D-00132.R2

Corresponding author: Professor Robert Bähring

Title: <i>KCND2</i> variants associated with global developmental delay differentially impair Kv4.2 channel gating

Colour figures: Yes

Dear Professor Bähring,

We are pleased to inform you that your paper has now been accepted for publication in Human Molecular Genetics and will appear in a forthcoming issue pending your acceptance of a licence to publish using our new online licensing system. The production editor will send you a link to this system and instructions to guide you through the process. Please note that this replaces the hardcopy forms which were formerly faxed and posted to the Oxford Journals Production department.

As soon as received you have accepted a licence to publish online, your manuscript will be published online as soon as possible through HMG Advance Access. In order to achieve this rapid publication time, the accepted manuscript is published online before copyediting and formatting has been carried out. Appearance in Advance Access constitutes official publication, and the Advance Access version can be cited by a unique DOI (Digital Object Identifier). Your manuscript will then be copyedited and typeset as normal, before print and online publication of the final version. Both versions of the paper will continue to be accessible and citable.

OPTIONAL OPEN ACCESS – HMG authors can opt, at an additional charge, to make their paper freely available online to all immediately upon publication, as part of the Oxford Open initiative.

If you wish to publish under an Open Access model, please select the Open Access licence in our online system, and complete the charge form once you have accepted the licence. Full instructions regarding this process will be sent by the production editor. Applicable Open Access charges can be found at <http://www.oxfordjournals.org/oxfordopen/#charges>.

If you do not select the Open Access option, your paper will be published in the journal with standard subscription-based access and you will not be charged.

Offprint order forms will be sent to you with your proofs. Sample offprint forms with cost details are available in the Author Centre of the submission website and on the journal website. Reprint requests notified to the publisher after the issue has gone to press will be charged extra to cover the additional printing cost.

Please note that if your paper contains colour figures or colour tables, there will be a cost for each, please visit the HMG website for more details at: http://www.oxfordjournals.org/our_journals/hmg_for_authors/general.html for specific costs.

Your manuscript is considered to be in its final form at this point. Only minor changes to correct errors in the text should be made at the proof stage. Changes to the figures should not be made and will only be allowed with prior permission from the Editors. Such changes may result in additional charges and/or delays in the publication of your paper.

Please note:

The Advance Access version of the article must be identical to that approved by the Editorial Office. All corrections should be made at the proof stage. The print-and online-versions of the articles must be identical. If colour figures are approved during the peer review process, they should be carried forward into the final printed article.

You will receive your official acceptance date from Oxford University Press once you have signed your licence to publish. (N.B. If you are a UK-based author and are looking to comply with the HEFCE policy on open access in the Research Excellence Framework, you should use the official acceptance date when depositing in your repository).

Thank you for publishing your work in Human Molecular Genetics.

Sincerely,

Professor Kay Davies
Executive Editor
Human Molecular Genetics
hmg.editorialoffice@oup.com

2 Presentation of the paper

2.1 Context of the study

2.1.1 Major new findings

Ion channels are crucial to maintain normal physiological functions of the body at the cellular and molecular level. Potassium channels play a very important role in regulating cell resting membrane potential and membrane repolarization, and they can be subdivided into various subtypes. Among these subtypes, voltage-gated potassium (Kv) channels are widely distributed in nerve and muscle tissues. In particular, rapidly inactivating (A-type) voltage-gated potassium (Kv4) channels mediate the subthreshold activating somatodendritic A-type current (I_{SA}) and the transient outward current (I_{to}), controlling the excitability of neurons and cardiac myocytes, respectively (Jerng et al. 2004, Patel and Campbell 2005). The human voltage-gated potassium channel gene subfamily D (*KCND*) has three members (*KCND1*, *KCND2* and *KCND3*), which encode three types of channel proteins, respectively (Kv4.1, Kv4.2 and Kv4.3). The molecular structure of Kv4 channel is basically clear: each protein (α -subunit) circuitously crosses the cell membrane 6 times generating 6 transmembrane segments, named S1-S6, with a P-loop sandwiched between S5 and S6, and every Kv4 channel complex has four α -subunits. This structure shares a high degree of conservation.

If Kv4 potassium channels are expressed in heterologous systems, the kinetic characteristics of activation and inactivation of the current are significantly different from those of native A-type current, suggesting that normally there are regulators or factors in the cytoplasm that play a regulatory role in the process of activation and inactivation of Kv4 channels (Maffie and Rudy 2008). In fact, potassium channel interacting proteins 1–4 (KCHIP1-4) with four 'EF-hand' like calcium binding motifs, were found to specifically bind to Kv4 potassium channels (An et al. 2000, Morohashi et al. 2002). KChIPs can increase the surface channel density, slow macroscopic inactivation, shift the voltage-dependent inactivation to the right and accelerate recovery from inactivation (An et al. 2000). In addition to KChIPs, dipeptidyl aminopeptidase-like proteins (DPPs) are also another kind of auxiliary subunit for Kv potassium channels, which are also important for channel gating dynamic characteristics and functional regulation. As reported, DPP6 modulates A-type currents by a variety of mechanisms: increase the cell membrane expression of Kv4.2 channel,

shift the voltage-dependent activation and inactivation to the left, and accelerate both macroscopic inactivation and recovery from inactivation (Nadal et al. 2003).

Recent data has found that the Kv4.2 channel is particularly important in the Kv4 family, and has a high density in the dendrites of pyramidal neurons (Hoffman et al. 1997), indicating the association between Kv4.2 channel function and neuronal networks. Genetic mutations, which can change channel functions and which are associated with disease pathogenesis, make people know more and more about the physiological importance of ion channel proteins. In the present paper a group of young individuals with global developmental delay (GDD) are shown to carry missense variants of *KCND2*, leading to single amino acid substitutions in Kv4.2.

Each of the individuals reported in the present paper carries one of the four mutations in Kv4.2: E323K, P403A, V404L, V404M. These amino acid substitutions are located in positions known to be critical for channel gating. To verify the hypothesis that the mutations critically affect Kv4.2 channel gating, particularly inactivation, the mutants were expressed in the *Xenopus* oocyte heterologous system and currents were measured under two electrode voltage clamp (TEVC).

There is one peculiar mutation (P403A) among the four *KCND2* variants, which is located in the second proline of the PVP motif that is likely to bend the helical S6 to allow gate opening and closing. The present paper confirms this notion, and it additionally shows that the PVP motif also plays a role in Kv4 channel inactivation, which corroborates the involvement of S6 motion in Kv4.2 channel inactivation. Intriguingly, substituting the valine residue directly following the PVP motif (V404L and V404M) left activation kinetics more or less unaffected, but still critically influenced Kv4.2 channel inactivation. As to the S4-S5 linker, E323K also showed impaired channel function, but the function could be rescued almost completely by KCHIP2 and DPP6.

The present paper supports the notion that the S4-S5 linker and the distal S6 segment play a particularly important role in Kv4.2 gating (Barghaan and Bähring 2009), and are instrumental in the installment of closed state inactivation (CSI). Although there is common agreement in the literature that Kv4 channels preferentially adopt CSI (Bähring and Covarrubias 2011), the molecular mechanism is still unclear. From a previous finding (left-shifted steady state inactivation curve for V404M; Lin et al. 2018), it had been concluded that a loss of contact between S4-S5 linker and S6 segment,

i.e., the previously proposed “uncoupling” (Barghaan and Bähring 2009), could not underlie CSI in Kv4.2 channels, because the side chain volume of methionine is larger than the one of valine. However, the present results and previously published ones suggest that side chain volume is not the major factor which determines CSI. In the present paper, although leucine (165 \AA^3) has the same side chain volume as methionine (168 \AA^3), the voltage dependence of inactivation has almost no shift in V404L mutant. Also, a previously studied V404A mutant (Barghaan and Bähring 2009), in which side chain volume was reduced from 139 to 90 \AA^3 , also displayed a negative shift in the voltage dependence of inactivation, which was even more obvious than observed for V404M in the present paper. In addition, there is another difference between the present paper and recent work (Lin et al. 2018). For E323K, the side chain was substituted to a positive charge which accelerated the recovery from inactivation, whereas the kinetics did not differ significantly between wild-type (WT) and E323D (Lin et al. 2018), suggesting that side chain charge at this position may be another influential factor of Kv4.2 channel gating. In a word, the present paper adds more complexity to the view published in the previous studies (Lee et al. 2014, Lin et al. 2018). More work is necessary to resolve the structural determinants of Kv4.2 channel CSI (see below § 2.1.3).

In order to judge the likely pathogenicity of the heterozygous *KCND2* mutations in the patient cohort, all the four Kv4.2 mutants were tested in a heteromeric ternary configuration (WT + mutant in the presence of both types of auxiliary subunits), which is referred to as the “native setting”. Many other potassium channel variants have been characterized previously, but in the present paper, it is the first time to test rigorously in a native setting. This may put some mutant effects into perspective because the mutant effects may be relativized or may even disappear due to the KChIP and/or DPP effects on channel expression and gating. A short description for all the mutants in the present paper is that they showed loss of function (LOF) and/or gain of function (GOF). WT+E323K ternary only had the LOF on the current size, while WT+P403A ternary had partial LOF and mixed with GOF. WT+V404M ternary only had GOF and WT+V404L had both.

Most of the known diseases related to Kv channel mutants including epilepsy (Allen et al. 2020) exhibit LOF which is much easier to reconcile with neuronal hyperexcitability, but several recent studies identified GOF variants associated with human epilepsy or

neurodevelopmental disorders, raising the possibility that enhanced K⁺ channel activity may also lead to hyperexcitability. Several explanations for the pathogenic GOF mechanisms are possible: (1) Kv channel GOF and reduced intrinsic excitability in inhibitory interneurons may lead to hyperexcitability in postsynaptic neurons (disinhibition); (2) Kv channel GOF and a resultant strong (after-) hyperpolarization following an action potential may remove sodium channel inactivation particularly well and, thus, lead to facilitated action potential firing; (3) Kv channel GOF leading to reduced activity of a neuron may increase the number of synapses and/or the number of postsynaptic glutamate receptors (homeostatic plasticity; Niday and Tzingounis 2018). In principle, the present paper agrees with the explanation given in a previous study (Lee et al. 2014) that disinhibition is responsible for epilepsy found in a V404M patient. The data of the present paper identify substitutions of V404 (both V404M and V404L) as a possible hot spot for epileptic seizure susceptibility.

GDD, as diagnosed for all the individuals in the present paper, is a disease characterized by obvious functional mental impairment and the deficiency of adaptability in social interaction, movement, cognition, language and other aspects. GDD applies to children younger than 5 years, who lag behind in two or more aspects of developmental functions significantly compared with children of the same age (Shevell et al. 2003). The etiologies of GDD are very complex, and the specific mechanism is still unclear. The results of the present paper strongly suggest that Kv4.2 channel GOF may be critically involved (see also Hamilton and Suri 2020).

Many studies have reported that *KCND* variants are associated with clinical phenotypes. For instance, GOF mutations in *KCND3* (Kv4.3) have previously been described in Brugada Syndrome (Giudicessi et al. 2011), and *KCND3*-pathogenic variants causing spinocerebellar ataxia type 19/22 introduce LOF (Smets et al. 2015). As for *KCND2* variants, one example is S447R, which was identified via analysis of whole-exome sequencing on 9 Jewish-Persian family members who suffered early-onset paroxysmal atrial fibrillation, exerted a GOF effect on Kv4.3 (Drabkin et al. 2018). Generally, all the previously published *KCND* variants seem to be that GOF causes cardiac phenotypes, whereas LOF causes neuronal phenotypes. But this trend is broken by the results of a recent publication (Lee et al. 2014) and the present paper, which both show that *KCND* GOF can also be related to neuronal phenotypes. The present paper raises a new finding that Kv4 dysfunction is not only related to epilepsy

and autism, but also to GDD, physical dysmorphology (see also Hamilton and Suri 2020) and developmental disorder in other aspects. However, there's a little bit of complexity about association between mutations and phenotypes. Although in case 4, 5 and 6 they have the same affected amino acid (V404), only case 4 suffers an autism. Coincidentally, only case 4 is male while case 5 and 6 are female. This also appeared on the previously reported autistic identical twin boys harboring the V404M variant (Lee et al. 2014). Taken together, it can therefore be assumed that gender is one of the factors that influences the genetic pre-disposition for autism. On the other hand, all the cases in the present paper exhibit a delayed motor and speech development together with a cognition problem, which can be seen as the key features associated with *KCND2* variants. Presumably, the exact clinical phenotypes a patient exhibits depends on the mutation in the protein (associated with either LOF or GOF or both), gender, early treatment, and probably other still unknown factors.

2.1.2 Limitations of the study

In the present paper, *Xenopus* oocytes are used as a heterologous expression system to study mutant effects on Kv4.2 channel function. Although oocytes have their own benefits, such as large in size, large in number and easy to manipulate and inject, there are still flaws that cannot be ignored. For instance, the endogenous ion channels in *Xenopus* oocytes may cause a contamination of the expressed channel current, especially for those mutants with tiny currents. Also, protein expression in *Xenopus* oocytes occurred at 16°C instead of 37°C (cell culture), which may have influenced the way channel proteins fold and assemble. Thus, the experimental results could have been reproduced in other heterologous expression systems, such as mammalian cell cultures (combined with whole cell patch clamp).

The reason for the reduced current amplitudes generated by P403A and E323K, even in the heteromeric ternary configuration, is still unclear. A possible explanation is that impaired channel trafficking and surface expression may contribute to the low current size. However, when using epitope-tagged Kv4.2 channels (external HA, C-terminal EGFP) combined with immunocytochemical methods to check the membrane expression of WT and these two mutants, no significant differences were found (experiments done by Claudia Schob, data not shown).

The present paper relies on the stoichiometry of channel subunits as defined by the amount of RNA injected. However, subunit assembly was not controlled, and

heteromer formation was not directly and convincingly shown, except for P403A, where the theoretical sum of WT and mutant currents clearly deviated from the measured currents. Notably also, in co-expression experiments biphasic curves were often obtained, raising the question whether the data were actually produced by one single channel population. Most strikingly, P403A exhibited a biphasic fitting curve of steady state inactivation reminiscent of two separate channel populations, which differ in their voltage dependences of inactivation. This issue was addressed by expressing P403A with KChIP2 at a 1:9 RNA ratio and measuring on the second day after injection to make sure all the KChIP2 RNA were expressed well, and all the channels were equally well complexed with KChIP2. Notably, the same biphasic fitting curve was obtained (data not shown), suggesting that this is an intrinsic feature of the P403A mutant channels in the presence of KChIP2. Due to the scope of the journal chosen for publication (Human Molecular Genetics), it seemed inappropriate to study this peculiar feature in more detail in the present paper.

The “native setting” in the present paper (Kv4.2 WT + mutant + KChIP2b + DPP6s) is arbitrary, and the real heteromers in the brain may be formed also with other Kv4 subtypes, other KChIPs and/or other DPPs. To test this issue, a brief check for the two particular channel mutants E323K and P403A has been done in the presence of different KChIPs (not mentioned in the present paper). It was found that, no matter which of the four KChIP subtypes was involved in ternary complex formation, WT + E323K heteromers almost completely resembled WT, whereas WT + P403A heteromers exhibited LOF with respect to the voltage dependence and kinetics of activation and the kinetics of recovery from inactivation, and GOF with respect to the voltage dependence and kinetics of inactivation and the kinetics of channel closure. Thus, the data obtained with different KChIPs resembled the ones published in the present paper.

The data generated in the present paper could have been used for a combined modeling approach, implementing Markov state models of Kv4.2 channel gating into more integrative models able to simulate cellular discharge behavior, based on the combination of gating models for all relevant channels. However, due to the lack of the necessary expertise, such global modeling was not performed in the present paper, and the Discussion had to remain hypothetical and speculative in many aspects.

Last but not least, it was not possible to develop an appropriate scoring system to correlate clinical phenotypes with a specific form of Kv4.2 channel dysfunction. Such a scoring system would allow for an accurate correlation between the genetic variants and clinical phenotypes.

2.1.3 Scientific and clinical outlook

Despite the limitations mentioned above, the results of the present paper will advance research in Kv4.2 channel biophysics and eventually bring benefits to patients with *KCND2* variants. A lot of experimental things still should be done in the future based on the present paper.

Much remains to be learnt regarding the molecular mechanisms that cause Kv4.2 channel dysfunction. One major push is to study clearly about the precise mechanisms of the CSI or channel gating process. The recent technique, patch clamp fluorometry, will be a good way to make it. This technique can combine the current with structure movement via showing with fluorescence. One can label the S4-S5 linker and S6 segment and once the physical interaction uncoupled, the fluorescence will change. Certainly, the interaction between the Kv4.2 mutants and auxiliary subunits also should be studied in more detail by using the same technique. In addition, cryogenic electron microscopy is an advanced technique to most directly study channel structure in a native environment. Also, more experiments should be done in order to verify the role of side chain volume on the interaction between S4-S5 linker and S6 segment. Based on the previously reported V404A and V404M, together with the V404 mutants in the present paper, more other substitutions should be tested in the future at this site to analyze systematic structure-function association. And also, P403A should be studied in more detail about the biphasic Boltzmann-curves.

Pharmacological treatment of epilepsy is based on two aspects: one is the inhibition of excitatory ligand and voltage-dependent ion channels and the inhibition of excitatory neurotransmitter release, the other is potentiation of GABAergic effects. The present paper may now open a novel opportunity for pharmacological interventions in developmental epileptic encephalopathy by targeting Kv4.2 channel in an appropriate manner, such as the inhibition of GOF. More pharmacological compounds, i.e., the tarantula toxins and the scorpion toxins, should be explored in more details to address their effectivity in neuronal and their tolerability in cardiac tissue, which could bring benefits to affected individuals.

Expressing all the mutants in cultured hippocampal neurons or expressing *KCND2* variants in transgenic mice would be a great method to study the mutants' dysfunctions in a real native setting. Animal models provide the opportunity to reproduce the growth process *in vivo*, and enable people to see the functional changes more intuitively through electrophysiological techniques, so as to explore the pathogenesis of nervous system diseases and drug research from the cellular and molecular levels. Since mouse genes are conserved with human, phenotypes of transgenic mice are also highly similar to those of human diseases, thus the relationship between mutated genes and diseases can be clearly studied.

From a clinical perspective, an advance in stem cell technology offers a way forward. Then the mutations can also be studied in a real native setting. Stem cell technology can provide a mean for assessing the pathophysiological mechanisms of individual Kv4.2 mutations (Zaydman et al. 2012).

2.2 References

- Allen, N.M., Weckhuysen, S., Gorman, K., King, M.D. and Lerche, H. (2020) Genetic potassium channel-associated epilepsies: clinical review of the Kv family. *Eur J Paediatr Neurol* 24, 105–116.
- An, W.F., Bowlby, M.R., Betty, M., Cao, J., Ling, H.P., Mendoza, G., Hinson, J.W., Mattsson, K.I., Strassle, B.W., Trimmer, J.S. and Rhodes, K.J. (2000) Modulation of A-type potassium channels by a family of calcium sensors. *Nature* 403 (6769), 553–556.
- Bähring, R. and Covarrubias, M. (2011) Mechanisms of closed-state inactivation in voltage-gated ion channels. *J Physiol* 589 (Pt 3), 461–479.
- Barghaan, J. and Bähring, R. (2009) Dynamic coupling of voltage sensor and gate involved in closed-state inactivation of Kv4.2 channels. *J Gen Physiol* 133 (2), 205–224.
- Drabkin, M., Zilberberg, N., Menahem, S., Mulla, W., Halperin, D., Yogev, Y., Wormser, O., Perez, Y., Kadir, R., Etzion, Y., Katz, A. and Birk, O.S. (2018) Nocturnal atrial fibrillation caused by mutation in *KCND2*, encoding pore-forming (α) subunit of the cardiac Kv4.2 potassium channel. *Circ Genom Precis Med* 11 (11), e002293.
- Giudicessi, J.R., Ye, D., Tester, D.J., Crotti, L., Mugione, A., Nesterenko, V.V., Albertson, R.M., Antzelevitch, C., Schwartz, P.J. and Ackerman, M.J. (2011) Transient outward current (I_{to}) gain-of-function mutations in the *KCND3*-encoded Kv4.3 potassium channel and brugada syndrome. *Heart Rhythm* 8 (7), 1024–1032.
- Hamilton, M.J. and Suri, M. (2020) ‘Electrifying dysmorphology’: potassium channelopathies causing dysmorphic syndromes. *Adv Genet* 105, 137–174.
- Hoffman, D.A., Magee, J.C., Colbert, C.M. and Johnston, D. (1997) K^+ channel regulation of signal propagation in dendrites of hippocampal pyramidal neurons. *Nature* 387 (6636), 869–875.
- Jerng, H.H., Pfaffinger, P.J. and Covarrubias, M. (2004) Molecular physiology and modulation of somatodendritic A-type potassium channels. *Mol Cell Neurosci* 27 (4), 343–369.
- Lee, H., Lin, M.C., Kornblum, H.I., Papazian, D.M. and Nelson, S.F. (2014) Exome sequencing identifies *de novo* gain of function missense mutation in *KCND2* in identical twins with autism and seizures that slows potassium channel inactivation. *Hum Mol Genet* 23 (13), 3481–3489.

- Lin, M.A., Cannon, S.C. and Papazian, D.M. (2018) Kv4.2 autism and epilepsy mutation enhances inactivation of closed channels but impairs access to inactivated state after opening. *Proc Natl Acad Sci U S A* 115 (15), E3559–E3568.
- Maffie, J. and Rudy, B. (2008) Weighing the evidence for a ternary protein complex mediating A-type K⁺ currents in neurons. *J Physiol* 586 (23), 5609–5623.
- Morohashi, Y., Hatano, N., Ohya, S., Takikawa, R., Watabiki, T., Takasugi, N., Imaizumi, Y., Tomita, T. and Iwatsubo, T. (2002) Molecular cloning and characterization of CALP/KChIP4, a novel EF-hand protein interacting with presenilin 2 and voltage-gated potassium channel subunit Kv4. *J Biol Chem* 277 (17), 14965–14975.
- Nadal, M.S., Ozaita, A., Amarillo, Y., Vega-Saenz de Miera, E., Ma, Y., Mo, W., Goldberg, E.M., Misumi, Y., Ikehara, Y., Neubert, T.A. and Rudy, B. (2003) The CD26-related dipeptidyl aminopeptidase-like protein DPPX is a critical component of neuronal A-type K⁺ channels. *Neuron* 37 (3), 449–461.
- Niday, Z. and Tzingounis, A.V. (2018) Potassium channel gain of function in epilepsy: an unresolved paradox. *Neuroscientist* 24 (4), 368–380.
- Patel, S.P. and Campbell, D.L. (2005) Transient outward potassium current, 'I_{to}', phenotypes in the mammalian left ventricle: underlying molecular, cellular and biophysical mechanisms. *J Physiol* 569 (Pt 1), 7–39.
- Shevell, M., Ashwal, S., Donley, D., Flint, J., Gingold, M., Hirtz, D., Majnemer, A., Noetzel, M., Sheth, R.D., Quality Standards Subcommittee of the American Academy of, N. and Practice Committee of the Child Neurology, S. (2003) Practice parameter: evaluation of the child with global developmental delay: report of the quality standards subcommittee of the american academy of neurology and the practice committee of the child neurology society. *Neurology* 60 (3), 367–380.
- Smets, K., Duarri, A., Deconinck, T., Ceulemans, B., van de Warrenburg, B.P., Züchner, S., Gonzalez, M.A., Schüle, R., Synofzik, M., Van der Aa, N., De Jonghe, P., Verbeek, D.S. and Baets, J. (2015) First *de novo* KCND3 mutation causes severe Kv4.3 channel dysfunction leading to early onset cerebellar ataxia, intellectual disability, oral apraxia and epilepsy. *BMC Med Genet* 16, 51.
- Zaydman, M.A., Silva, J.R. and Cui, J. (2012) Ion channel associated diseases: overview of molecular mechanisms. *Chem Rev* 112 (12), 6319–6333.

3 Summary

Four *KCND2* missense variants, identified in six unrelated individuals with early onset GDD, were functionally characterized. For this purpose, the respective Kv4.2 mutants with single amino acid substitutions, all at functionally relevant sites (E323K, P403A, V404L and V404M), were expressed in a heterologous system, and the currents were measured under two electrode voltage clamp. The mutant channels showed characteristic gating modifications both in the absence and presence of the auxiliary β -subunits KChIP2 and DPP6, and auxiliary β -subunit co-expression augmented the functional expression of both WT and mutant channels. In the heteromeric ternary configuration (co-expression of WT + mutant and simultaneous co-expression of both KChIP and DPP), which is referred to as the “native setting”, E323K displayed mild LOF, P403A and V404L a mixture of partial LOF and GOF features, and V404M only GOF features. The results of the present paper corroborate the functional importance of the S4-S5 linker and the distal S6 segment in Kv4.2 channel inactivation, they indicate a critical involvement of Kv4.2 channel dysfunction in the etiology of GDD, and they identify substitutions of V404 as likely determinants of epileptic seizure susceptibility. Thus, the present paper will support the development of early mechanism-based precision medicine to benefit young individuals and minimize developmental disturbances.

4 Zusammenfassung

Es wurden vier *KCND2*-Missense-Varianten von insgesamt sechs nicht verwandten Individuen mit globaler Entwicklungsverzögerung funktionell charakterisiert. Zu diesem Zweck wurden die entsprechenden Kv4.2-Mutanten mit einzelnen Aminosäure-Substitutionen, alle an funktionell relevanten Stellen (E323K, P403A, V404L und V404M), in einem heterologen System exprimiert, und die Ströme wurden mittels Zwei-Elektroden-Voltage-Clamp gemessen. Die mutierten Kanäle zeigten sowohl in der Abwesenheit als auch in der Anwesenheit der akzessorischen β -Untereinheiten KChIP2 und DPP6 charakteristische Veränderungen im Gating, und die Coexpression akzessorischer β -Untereinheiten erhöhte die funktionelle Expression sowohl von Wildtyp- als auch von mutierten Kanälen. In der heteromeren ternären Konfiguration (Coexpression von WT + Mutante und gleichzeitige Coexpression von sowohl KChIP2 als auch DPP6), hier als „native Situation“ bezeichnet, zeigte E323K einen milden LOF, P403A und V404L eine Mischung aus partiellen LOF- und GOF-Eigenschaften, und V404M ausschließlich GOF-Eigenschaften. Die Ergebnisse der vorliegenden Arbeit untermauern die funktionelle Bedeutung des S4-S5-Linkers und des distalen S6-Segments für die Kv4.2-Kanalinaktivierung, sie deuten auf eine entscheidende Beteiligung einer Kv4.2-Kanaldysfunktion bei der Ätiologie globaler Entwicklungsverzögerungen hin, und sie identifizieren Austausche von V404 als wahrscheinliche Determinanten für eine erhöhte Wahrscheinlichkeit epileptischer Anfälle. Somit wird die vorliegende Arbeit die Entwicklung einer frühzeitigen mechanismus-basierten Präzisionsmedizin unterstützen, zum Nutzen junger Individuen, und um Entwicklungsstörungen zu minimieren.

5 Declaration of own contribution

The present paper is based on a collaborative effort with a large number of authors and institutions. I contributed the following:

- Study concept (discussion of co-expression strategies, experimental conditions and voltage protocols)
- Heterologous channel expression (frog surgery assistance, oocyte preparation, RNA synthesis, RNA injection)
- Electrophysiological experiments (preparation of recording solutions and electrodes, TEVC recordings)
- Data analysis (analysis of raw data, plotting data, fitting mathematical functions to the data, statistical analysis)
- Publication (draft contributions, summary tables, proof-reading)

6 Acknowledgements

In the first place, I want to sincerely thank my mentor Prof. Dr. Robert Bähring. It is no exaggeration to say he is the best teacher I have met till now. He helps me a lot not only in my study but also in my life, which let me really understand that teacher can also be a good friend. In terms of study, he has always been patient enough to guide me, and can give timely and accurate answers to all my questions, even one question was asked for several times. What has benefited me most is his attitude towards scientific research. He is meticulous about all scientific research issues, and can always find reasonable and correct explanations and conjectures after searching literatures, and take actions to verify them. I am very honored to be his student.

And then I'd like to thank the China Scholarship Council (CSC). Without its full economic support, I would not have been able to successfully complete my doctoral study in Germany. Every year, the China Scholarship Council supports thousands of students to study abroad, which makes me feel China's selfless dedication to talent education without asking for anything in return. This is really touching.

One tree does not make a forest. My colleagues in our institute also provided me with a lot of help, such as Tassja, Claudia, Peter, Helga, Christiane, Annett, et al. Especially Georgios Tachtsidis, he really gave me a lot of help. We often discuss together and I ask him many questions about our thesis, then he always gives me serious and careful answers. Not only that, he always takes the trouble to help me deal with all kinds of things that need German, such as: extending my residence permit, making phone calls, replying emails. He is one of my best friends in Germany.

Finally, a heartfelt thank you also goes to my families, especially for my wife, Jing Wei. She paid a lot, because she quit her job as a nurse in China and came to Germany alone to be with me. In these three years, she is always by my side, no matter I am happy or sad, always bear my temper, relieve the pressure of life for me, and give me encouragement and support, so that I can always concentrate on my work.

7 Curriculum Vitae

Personal Information

Name: Yongqiang Zhang

Date of Birth: 19.04.1992

Gender: Male

Nationality: Chinese

Email: y.zhang.ext@uke.de; qq807049434@163.com

Telephone: +49 015227635255; +86 15851865896

Educational Background

Dec, 2018: Start of MD study at University Medical Center Hamburg-Eppendorf, Hamburg, Germany

Sep, 2016-Jul, 2018: Master of Clinical Medicine, Southeast University, Nanjing, PR of China

Sep, 2011-Jul, 2016: Bachelor of Clinical Medicine, Southeast University, Nanjing, PR of China

Awards and Honors

Scholarship from China Scholarship Council; China Scholarship Council, 2018.

Outstanding intern in school of medicine; Southeast University, 2016

Award of the nasogastric tube insertion in Clinical Skills Competition in school of medicine; Southeast University, 2016

Xuzhou alumni Scholarship, 2013

Academic Publications:

Zhang, Y., Tachtsidis, G., Schob, C., Koko, M., Hedrich, U.B.S., Lerche, H., Lemke, J.R., Haeringen, A., Ruivenkamp, C., Prescott, T., Tveten, K., Gerstner, T., Pruniski, B., DiTroia, S., VanNoy, G.E., Rehm, H.L., McLaughlin, H., Bolz, H.J., Zechner, U., Bryant, E., McDonough, T., Kindler, S. and Bähring, R. (2021) *KCND2* variants associated with global developmental delay differentially impair Kv4.2 channel gating. *Hum Mol Genet* (in press)

Zhang, Y., Li, Y., Liu, H., Bai, J., Bao, N., Zhang, Y., He, P., Zhao, J., Tao, L., Xue, F., Zhou, G. and Fan, G. (2018) Mechanical and biological properties of a biodegradable Mg-Zn-Ca porous alloy. *Orthop Surg* 10 (2), 160–168.

8 Eidesstattliche Versicherung

Ich versichere ausdrücklich, dass ich die Arbeit selbständig und ohne fremde Hilfe verfasst, andere als die von mir angegebenen Quellen und Hilfsmittel nicht benutzt und die aus den benutzten Werken wörtlich oder inhaltlich entnommenen Stellen einzeln nach Ausgabe (Auflage und Jahr des Erscheinens), Band und Seite des benutzten Werkes kenntlich gemacht habe.

Ferner versichere ich, dass ich die Dissertation bisher nicht einem Fachvertreter an einer anderen Hochschule zur Überprüfung vorgelegt oder mich anderweitig um Zulassung zur Promotion beworben habe.

Ich erkläre mich einverstanden, dass meine Dissertation vom Dekanat der Medizinischen Fakultät mit einer gängigen Software zur Erkennung von Plagiaten überprüft werden kann.

Unterschrift: 